Heliyon 10 (2024) e31118

Contents lists available at ScienceDirect

Heliyon

journal homepage: www.cell.com/heliyon

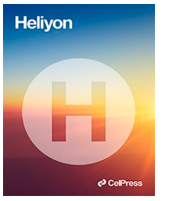

Review article

Recent advances in multifunctional electromagnetic interference shielding materials

Quy-Dat Nguyen [a,b], Choon-Gi Choi [a,b,*]

[a] Graphene Research Team, Materials and Components Research Division, Superintelligence Creative Research Laboratory, Electronics and Telecommunication Research Institute (ETRI), Daejeon, 34129, Republic of Korea
[b] Semiconductor and Advanced Device Engineering, ETRI School, University of Science and Technology (UST), Daejeon, 34113, Republic of Korea

ARTICLE INFO

Keywords:
Multifunction
Electromagnetic interference shielding
MXene
Sensing
Heating
Thermal management

ABSTRACT

Electromagnetic interference (EMI) shielding material is the most effective solution to protect electronic devices and human health from the harmful effects of electromagnetic radiation. The study of EMI shielding materials is intensifying in the constantly developing picture of the fourth industrial revolution. Many EMI shielding materials based on metal, carbon, emerging MXene materials, and their composites have been discovered to utilize the EMI shielding performance. However, a huge demand for compact and multi-functional devices requires the integration of new functions into EMI shielding materials. Multifunctional EMI shielding materials perform multiple functions beyond their main function of EMI shielding in a system due to their specific properties. The additional functions can either naturally exist or be specially engineered. This review summarizes the recent progress of cutting-edge multifunctional EMI shielding materials. The possibility of combining multifunction EMI shielding materials, such as strain sensing, humidity sensing, temperature sensing, thermal management, etc., and the difficulties in balancing EMI shielding performance with other functions are also discussed. Lastly, we point out challenges and propose future directions to develop research on multifunctional EMI shielding materials.

1. Introduction

The fifth-generation (5G) technology in telecommunications is no longer strange to the world, and even the next generation, the sixth-generation (6G) technology, has been interested and is currently under development [1]. It cannot be denied that modern technology brings immeasurable benefits, but its downside cannot be underestimated. Electromagnetic wave pollution is one of the major concerns as wireless connectivity and electronic devices evolve. Electromagnetic wave pollution causes interference that distorts the accuracy of nearby electronic devices and threatens human health [2,3]. Consequently, demand for EMI shielding materials is growing intensively.

Research directions on EMI shielding have been rapidly increasing over the past 15 years. High EMI shielding effectiveness (EMI SE) [4], thin thickness [4], lightweight [5], good mechanical properties [6], flexibility [7], efficient manufacturing [8], low cost [8], etc. Are often prioritized for EMI shielding materials. However, as the demand for compact and multi-functional devices rises, there is a

* Corresponding author. Graphene Research Team, Materials and Components Research Division, Superintelligence Creative Research Laboratory, Electronics and Telecommunication Research Institute (ETRI), Daejeon, 34129, Republic of Korea.
E-mail addresses: dat.nguyenquy.mse@etri.re.kr (Q.-D. Nguyen), cgchoi@etri.re.kr (C.-G. Choi).

https://doi.org/10.1016/j.heliyon.2024.e31118
Received 18 January 2024; Received in revised form 9 May 2024; Accepted 10 May 2024
Available online 11 May 2024

growing trend toward researching EMI shielding materials that integrate new functions. Multifunctional EMI shielding materials refer to materials that perform multiple functions beyond their primary role of EMI shielding due to their specific properties. These additional functions can either naturally exist or be specially engineered. The incorporation of new functionalities into EMI shielding materials expands their application scenarios.

For example, EMI shielding with thermal dissipation can be potentially applied to spacecraft materials and aerospace applications [2]. Highly thermally conductive EMI shielding materials are utilized in small and high-frequency devices to prevent EMI and enhance heat dissipation, guaranteeing efficient and precise operation [3]. The multifunctional EMI shielding fabrics presented by Zhang et al. are purportedly able to be made into clothes for soldiers or civilians [9]. These multifunctional EMI shielding garments can not only shield individuals from EM radiation but also provide warmth in cold environments owing to the Joule heating function. Furthermore, a body health monitoring capability was added to this multifunctional EMI shielding fabric. The authors proposed a concept of smart clothing that both protects the wearer from EM wave pollution and monitors heart rate owing to the strain sensing function [9]. In addition, many useful features have been incorporated into multifunctional EMI shielding materials. The selection of additional functions to integrate into the multifunctional EMI shielding material depends on the composition materials and the desired features, which will be explained in more detail in the main body of this report.

Through a survey of research related to multifunctional EMI shielding materials, we found that the research achievements in this direction are very significant. However, a comprehensive report on multifunctional EMI shielding materials has yet to be published. Therefore, we hope that, through our study on recent advances in multifunctional EMI shielding materials, readers can gain an overview of this promising research direction. Besides, an explanation of the mechanism involved between EMI shielding and additional functions is provided, and perspectives for further research are also suggested.

This review focuses on additional functions of material beyond the main property of EMI shielding, including strain sensing, humidity sensing, temperature sensing, heating, and others, which are discussed in detail in Section 3. Before that, for the convenience of readers, the principle of EMI shielding and an overview of the state of the art in recent EMI shielding materials are presented in Section 2. Lastly, the challenges and prospects of multifunctional EMI shielding materials are discussed in Section 4.

2. EMI shielding function

2.1. EMI shielding fundamentals

The mechanism of EMI shielding based on conductive materials is explained in Fig. 1. When propagating in a medium, the electric and magnetic fields of EM waves can be expressed as [10]:

$$\overrightarrow{E} = Ee^{-\gamma z}\hat{a}_x = Ee^{-\alpha z}e^{-j\beta z}\hat{a}_x = Ee^{-\alpha z}(\cos\beta z - j\sin\beta z)\hat{a}_x \quad (1)$$

$$\overrightarrow{H} = He^{-\gamma z}\hat{a}_y = He^{-\alpha z}e^{-j\beta z}\hat{a}_y = He^{-\alpha z}(\cos\beta z - j\sin\beta z)\hat{a}_y \quad (2)$$

where γ is the propagation constant of the medium, α is the attenuation constant, β is the phase shift constant, and E and H are the amplitudes of the electric and magnetic fields. If an EM wave is incident at the interface of two different media, reflection may occur:

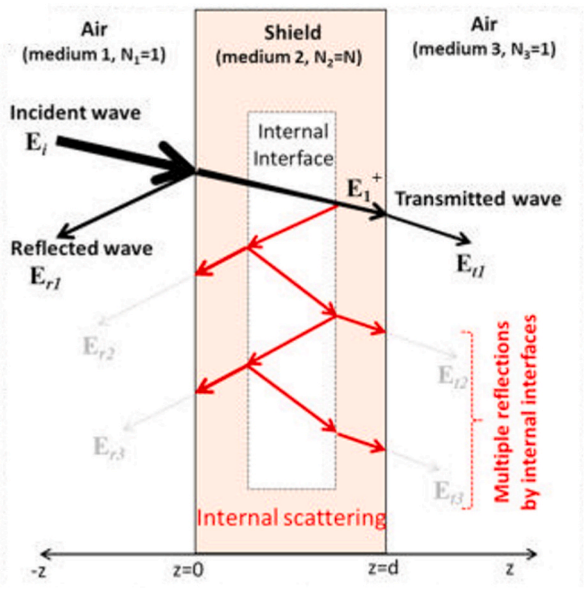

Fig. 1. EMI shielding mechanism in materials. Reproduced with permission from Ref. [11]. Copyright 2020 The Authors. Published by Elsevier Ltd.

$$R_{12} = \frac{E_r}{E_i} = \frac{n_2 - n_1}{n_2 + n_1} \tag{3}$$

$$T_{12} = \frac{E_t}{E_i} = \frac{2n_2}{n_2 + n_1} \tag{4}$$

R is reflection coefficient, T is transmission coefficient, n is impedance

$$n = \frac{|E|}{|H|} = \sqrt{\frac{j\omega\mu}{\sigma + j\omega\varepsilon}} \tag{5}$$

Where ω is angular frequency, μ is magnetic permeability, σ is electrical conductivity, and ε is permittivity. Because medium 2 is a shield (conductive, lossy medium $\alpha > 0$), the lossy medium absorbs the wave:

$$E_2 = E_0 e^{-\alpha z} \tag{6}$$

The formula of attenuation constant is:

$$\alpha = \omega \sqrt{\frac{\mu\varepsilon}{2}\left[\sqrt{1 + \left(\frac{\sigma}{\omega\varepsilon}\right)^2} - 1\right]} \tag{7}$$

The ratio of the total transmission to the incident of the shield can be expressed:

$$\frac{E_t}{E_i} = T_{12} e^{-\alpha d} T_{23} = \frac{2n}{n + n_0} e^{-\alpha d} \frac{2n_0}{n + n_0} = \frac{4nn_0}{(n + n_0)^2} e^{-\alpha d} \tag{8}$$

where d is the thickness of the shield. The total shielding effectiveness (SE_T) of the shield in dB is calculated as:

$$SE_T = 20\ log\left(\frac{E_i}{E_t}\right) \tag{9}$$

$$SE_T = SE_R + SE_A = 20\ log\frac{(n + n_0)^2}{4nn_0} + 20\ log\ \ e^{\alpha d} \tag{10}$$

where SE_R is the shielding due to reflection, SE_A is the shielding due to absorption. For electrically conductive shield materials $\sigma \gg \omega\varepsilon$ therefore

$$\alpha = \sqrt{\pi f \mu \sigma} \tag{11}$$

$$n = \sqrt{\frac{j\omega\mu}{\sigma}} = \sqrt{\frac{j2\pi f\mu}{\sigma}} \tag{12}$$

If medium 1 and 3 are air, then:

$$n_1 = n_3 = n_0 = \sqrt{\frac{\mu_0}{\varepsilon_0}} = 377\ \Omega \tag{13}$$

Therefore,

$$SE_R = 39.5 + 10\ log\frac{\sigma}{2\pi f\mu} \tag{14}$$

$$SE_A = 8.7\alpha d = 8.7\frac{d}{\delta} = 8.7d\sqrt{\pi f\mu\sigma} \tag{15}$$

Here, δ is defined as the skin (or penetration) depth, which means the distance at which the intensity of the electric field decreases to 1/e

$$\delta = \frac{1}{\alpha} = \frac{1}{\sqrt{\pi f\mu\sigma}} \tag{16}$$

Through surveying, most reports on EMI shielding conduct EMI shielding measurement by recording scattering parameters (S parameters) from vector network analyzers (VNA) systems. The incident and transmitted EM waves can be expressed in both two ports of the VNA (S_{11} and S_{12} and their reciprocals, S_{22} and S_{21} S parameters of the samples were measured by a vector network analyzer in the frequency ranges). With VNA, depending on the frequency range, sample size, special requirements, etc. There are three most common measurement techniques, including (1) the co-axial cable method, (2) the waveguide method, and (3) the free space method.

All the methods mentioned above give data as S parameters to calculate EMI shielding as follows. The reflection (R), transmission (T), and absorption (A) coefficients can be calculated according to:

$$T = |S_{21}|^2 = |S_{12}|^2 \tag{17}$$

$$R = |S_{11}|^2 = |S_{22}|^2 \tag{18}$$

Shielding effectiveness can be calculated as below:

$$SE_{Total}(dB) = SE_R(dB) + SE_A(dB) \tag{19}$$

$$SE_R(dB) = -10\,log(1-R) \tag{20}$$

$$SE_{Total}(dB) = -10\,log(T) \tag{21}$$

$$SE_A(dB) = SE_{Total}(dB) - SE_R(dB) \tag{22}$$

SE_{Total} is total shielding effectiveness; SE_A is shielding effectiveness by absorption; SE_R is shielding effectiveness by reflectance.

In addition, the EMI shielding performance of a material can be evaluated, taking into consideration the thickness (t) and weight of the material. Hence, specific EMI shielding effectiveness (SSE) and absolute EMI shielding effectiveness (SSE/t) are identified as below [12]:

$$\text{SSE} = \text{EMI SE/density} = \text{dB cm}^3\ \text{g}^{-1} \tag{23}$$

$$\text{SSE/t} = \text{SSE}_t = \text{EMI SE/density/t} = \text{dB cm}^2\ \text{g}^{-1} \tag{24}$$

2.2. Recent advances in EMI shielding materials

EMI shielding materials are often based on metal, carbon materials, and the most recent MXene materials. It can be a single material or a combination of two or more materials. In this part, we express the advances in EMI shielding materials based on main materials including metal-based, carbon-based (carbon nanotube and graphene), and MXene-based materials.

2.2.1. Metal based EMI shielding materials

Due to their outstanding electrical conductivity, metals such as silver (6.8×10^5 S/m), copper (6.4×10^5 S/m), aluminum (4.0×10^5 S/m), and magnetic metals such as nickel (9.7×10^4 S/m) and steel (6.3×10^4 S/m) are the most common EMI shielding materials [13]. The comparison of the EMI shielding performance of metal-based EMI shielding materials is shown in Table 1. Reflection and absorption of EM waves dominate EMI shielding performance because of the abundance of free electrons in the lattice of metal.

The most traditional EMI shielding materials are rigid metals. Song et al. reported a 2 mm-thick magnesium sheet (Mg–3%Al–1%

Table 1
Comparison of EMI shielding performance of metal-based EMI shielding materials.

Material	Filler content (wt%)	Thickness (mm)	Frequency (GHz)	SE_T (dB)	Ref.
Mg–3%Al–1%Zn alloy	100	2	0.03–1.5	88–98	[14]
Mg–Zn–Zr–Ce alloy	100	2	1.2	71	[15]
Mg–Y–Zn alloy	100	2	0.6	80–95	[16]
Mg–Fe composite	100	2	8.2–12.4	75	[17]
NiFe/Cu multi-layer	100	0.004	0.7–10	80–90	[18]
Al foam	100	10	0.13–1.8	45–75	[19]
Al foam	100	2.5	8.2–12.4	44.6	[20]
Ti/Ni foam	100	9	0.3–400 MHz	25–72	[21]
Cu coated textile	–	–	0.1–1	35–50	[22]
CF/PPy/Cu	–	–	0.03–1	30.3–50.4	[23]
Cu/bamboo fabric	–	–	0.0002–1	40–55	[24]
AgNPs/wrinkled textile	20	–	8.2–12.4	101.1	[25]
SSF/PET fabric	40	0.5	0.03–1.5	~40	[26]
Ni coated carbon fiber/ABS composite	–	–	0.03–1	30	[27]
Natural fiber-resin/Al	–	–	8–12	28.5–53.5	[28]
P@Ni–Co alloy	–	0.18	8–26.5	77.8	[29]
CuNW/PS	13	0.21	8.2–12.4	42	[30]
AgNW/Cellulose	9.57	5	1	48.6	[31]
CA/AgNW/PU	–	–	8.2–12.4	31.3	[32]
PES/AgNW/PET	–	–	8–12	~30–40	[33]
Ag/PLA	7.75	2.7	8.2–12.4	60.4	[34]
FeSiAl/metal hybrid	60	3	300 kHz-10	65.6	[35]

Zn) with an EMI SE of 88–98 dB at a frequency of 30–1500 MHz [14]. Liu et al. prepared Mg–Zn–Zr–Ce alloys, showing a superior EMI SE of 71 dB at frequency 1.2 GHz [15], and Mg–Y–Zn ternary alloys with various ratios of Y and Zn in the alloy, showing an ultrahigh EMI SE of 80–95 dB [16]. A magnesium-iron micro-composite was prepared using the disintegrated melt deposition (DMD) technique [17]. Iron micro-particles (size 74 μm) were uniformly dispersed in magnesium molten and then molded into an EMI shielding disc, achieving an EMI SE of ~75 dB with a thickness of 2 mm. Metal-based EMI shielding materials can be fabricated as thin films through deposition methods. Park et al. deposited Cu and NiFe on 50 nm Ti to obtain 4 μm thickness films of pure Cu/Ti, pure NiFe/Ti, and multilayer NiFe–Cu/Ti by DC magnetron sputtering [18]. After investigation of EMI shielding performance, the multilayer NiFe–Cu/Ti was demonstrated to be more efficient with an EMI SE of 80–90 dB in the frequency range of 0.7 GHz–10 GHz, attributed to multiple reflections at the NiFe/Cu interfaces.

To overcome the disadvantages of heavy weight and enhance the efficiency of EMI shielding, metal foams have been developed. Xu et al. investigated the effect of porosity on the EMI shielding performance of aluminum foams [19]. With the increase from 75.61 to 93.08 %, the EMI SE initially remained and then increased to reach a maximum of 75 dB in the frequency range of 130 MHz–1800 MHz. Kumar et al. fabricated an aluminum foam using the replica impregnation technique [20]. A polyurethane foam was dipped in an aluminum slurry to form an aluminum-impregnated PU foam before being removed through sintering to obtain an aluminum foam. The foam with a thickness of 2.5 mm showed an excellent EMI SE of 44.6 dB in the frequency range of 8.2–12.4 GHz due to enhancing multiple scattering EM waves, as shown in Fig. 2a. Similarly, Liu et al. also used an impregnation method with a PU template to prepare a metal foam of titanium/nickel [21]. The sample with a thickness of 9 mm showed an EMI SE of 25–72 dB in the frequency range of 0.3–400 MHz.

Metal-coated fabrics are often popular for EMI shielding textiles owing to their high electrical conductivity and flexibility. Via the electroless plating technique, Lu et al. deposited copper on modal fabric (Cu/MF), prepared multilayer structured cuprammonium fabric/polypyrrole/copper (CF/PPy/Cu) composites, and fabricated copper/bamboo fabric (Cu/BF) composites [22–24]. These fabrics exhibited high EMI SE and good durability, as proven by washing and mechanical tests. Yang et al. reported that coating silver nanoparticles (AgNPs) on modified wrinkled textiles (Ag_nPWT) can improve EMI shielding performance [25]. When increasing the coating solution of AgNPs from 2.5 mg/ml to 20 mg/ml, the silver-coated textile composite achieved EMI SE from 24.5 dB to 101.1 dB, respectively, as illustrated in Fig. 2b. This significant enhancement of EMI SE was due to the improvement of the consecutive conductive Ag network formed on the wrinkled textile. The addition of ingredients to improve conductivity and magnetic loss from soft metallic magnetic materials also helps to enhance the EMI shielding performance of fabrics. 316L stainless steel fibers, which are molybdenum-bearing low-carbon austenitic stainless steel, were blended with polyester fibers (PET) to form an SSF/PET yarn [26]. The textile achieved an EMI SE of ~40 dB at 0.5 mm thick with 40 wt% SSF.

Metals are combined with polymer matrices or fibers to form conductive composites that can dissipate the energy from EM waves. Tzeng & Chang prepared nickel-coated carbon fibers by electroless deposition techniques, then reinforced these fibers in ABS composites [27]. The EMI SE of the composite is as high as ~30 dB in the frequency range of 30–1000 MHz due to excellent adhesion

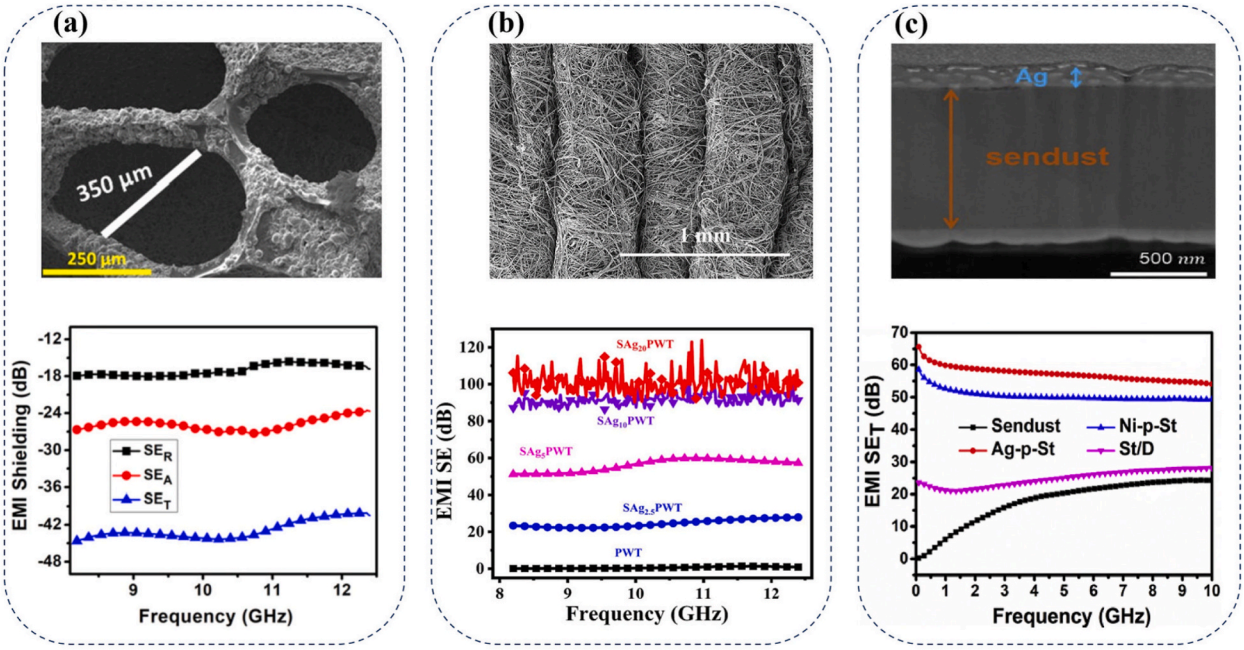

Fig. 2. Metal-based EMI shielding materials. SEM image of the microstructure and EMI SE performance of (a) Al foam. Reproduced with permission from Ref. [20]. Copyright 2019 Elsevier B.V. (b) AgNP/wrinkled textile composite. Reproduced with permission from Ref. [25]. Copyright 2023 Elsevier B.V. (c) Ag-plated sendust (Ag-p-St) hybrid composites. Reproduced with permission from Ref. [35]. Copyright 2019 Elsevier Ltd.

between the nickel coating layer and the carbon fibers. In a report by Xia et al., two aluminum sheets (thickness of 24 μm) were sandwiched between three layers of natural fiber-resin through a vacuum-assisted resin transfer molding (VARTM) process to form a multilayer EMI shield [28]. The EMI SE values of the shield achieved 28.5–53.5 dB in the frequency range of 8–12 GHz with good mechanical properties. To obtain a low-density, flexible, and high-EMI shielding performance material, Zhang et al. electrospun PAN-PU/Ag fibers into a membrane and then electroless plated Ni–Co alloy nanoparticles to form a P@Ni–Co hybrid membrane [29]. The EMI SE of the membrane is as high as 77.8 dB in a wide frequency range (X-band, Ku-band, and K-band), owing to its high electrical conductivity and good magnetic properties.

With their tiny sizes, metal nanomaterials, such as nanoparticles and nanowires, play roles as fillers in polymer nanocomposites. In these polymer composites, the percolation threshold, which is the critical content of metal nanomaterials indicating the transition from an insulator to a conductor, is an important parameter. Therefore, the conductivity and EMI shielding performance can be significantly enhanced if the composites possess a low percolation threshold. Sundararaj et al. reported a novel method for the preparation of nanocomposites known as miscible solvent mixing and precipitation (MSMP) [30]. By this method, copper nanowires (CuNW) with

Table 2
Comparison of EMI shielding performance of carbon-based EMI shielding materials.

Material	Filler content (wt%)	Thickness (mm)	Frequency (GHz)	SE_T (dB)	Ref.
PVDF/MWCNTs	7	2	8.2–12.4	30.89	[36]
MWCNT/WPU	10.6	0.4	8.2–12.4	24.7	[37]
PLLA/MWCNT	1.1	1.5	8.2–12.4	30	[38]
CNT/NR	70	0.25	8.2–12.4	44.7	[39]
MWCNT/polycarbonate	5	1.85	8.2–12.4	25	[40]
MWCNT/polystyrene	5	2	8.2–12.4	11.46	[41]
MWCNT/ABS	10	–	12.4–18	39	[42]
MWCNT/PPCP	4.6 vol%	2	12.4–18	48	[43]
CNT/PE	5	2.1	8.2–12.4	46.4	[44]
PMMA wrapped MWCNT/PVDF/ABS	3	5.6	8–18	32	[45]
PLA/MWCNT	3	2	8.2–12.4	31.02	[46]
CNT/PP	5	2.2	8.2–12.4	48.3	[47]
CNT/UHMWPE	4	1.6	8–18	32.6	[48]
CNT/UHMWPE	2	1	8–18	33.5	[49]
iPP/POE/MWCNTs	3	1.2	8–12	25	[50]
Ni/MWCNT/HDPE	–	3	0.5–1.5	16	[51]
Ni/MWCNT/Epoxy	–	1	0.5–1	4–6.5	[52]
Epoxy-MWCNT/Fe_3O_4	10	3	13–40	>40	[53]
PVDF/MWCNT/Ni–Fe	53	2.5	8–12	35	[54]
MWCNT/NdFeB/Epoxy	35	1.1	8.2–12.4	34.09	[55]
Au@CNT/SA/PDMS	6	2	8–12	60	[56]
Au-decorated densified CNT	100	0.0143	8.2–12.4	71	[57]
Coupled CNT	100	0.023	8.2–12.4	78	[58]
PC/GNP	6	1	8.2–12.4	35	[59]
P(St-BA)/S-rLGO	25	0.25	8.2–12.4	15.9	[60]
P(St-BA)/S-GNS	25	1.8	8.2–12.4	71.5	[61]
GN/WPU	5	–	8.2–12.4	38	[62]
rGO/WPU	7.5	1	8.2–12.4	34	[63]
rGO/PP	20	2	8–18	50	[64]
SR/Graphene	3	1.7	8.2–12.4	34.72	[65]
NBR/GN	4	2	1–12	77	[66]
Ag@FRGO/WPU	5	2	8.2–12.4	35	[67]
TGO/SCI/Epoxy	33	4	11.7	40	[68]
G-Ni/PC/SAN	3	–	18	29.4	[69]
GNP/Ni/Wax	30	0.7	8–12	40	[70]
Ni@Graphene-PVDF	20	0.7	18–26.5	51.4	[71]
PVDF/Carbon/Ni	13	0.6	18–26.5	55.8	[72]
GNSs-Fe_3O_4/PVDF	13.3 vol	0.3	8.2–12.4	52	[73]
PS/TGO/Fe_3O_4	2.24	–	9.8–12	30	[74]
RGO@Fe_3O_4	8.97	2	8.2–12.4	13.45	[75]
Fe_3O_4@rGO/NR	10	1.8	8.2–12.4	37	[76]
$NiFe_2O_4$-RGO-Elastomer	5	2	5.85–8.2	28.5	[77]
GNP/CLF/PEEK	2.5	2.5	8.2–12.4	27.1	[78]
RGO/c-Fe_2O_3/C	38	0.4	8.2–12.4	42.83	[79]
PC/GNP/MWCNT	4	5.6	8.2–12.4	21.6	[80]
PVA/MWCNT-Graphene	10	1	1–2	32.89	[81]
GCNT/WPU	10	3	12.4–18	47	[82]
r-OCNTs/TG/PDMS cake	–	1	8.2–12.4	67.3	[83]
rGO/MWCNT/PDMS	0.98	2.4	8.2–12.4	56	[84]
PC/MWCNT/GO/MnO_2	8	0.9	8–18	57	[85]
G-CNT-Fe_2O_3	–	0.1	8–12	134	[86]
Fe_3O_4@AGA/EP	0.36	–	12.4	40.4	[87]
PDMS/FRS/RGO-SWCNH	11	10	14.5–20	34.83	[88]

high aspect ratios formed a segregated structure in the polystyrene (PS) matrix, leading to a composite with a low percolation threshold of 0.67 vol%. Hence, the CuNW/PS composite with a copper concentration of only 1.3 vol% possessed a high electrical conductivity of 10^4 S m^{-1}, resulting in a high EMI SE of more than 20 dB even though the thickness of the film is only 0.21 mm. Lee et al. reported a silver nanowire (AgNW)-coated cellulose paper fabricated by a facile dip-coating method [31]. AgNW is distributed in a hierarchical structure, with density gradually reducing in the thickness direction of the cellulose paper, resulting in anisotropic apparent electrical conductivity. The AgNW/cellulose paper, composed of only 9.57 wt% AgNW content, exhibited a high EMI SE of 48.6 dB with a thickness of 160 μm at 1 GHz. AgNW was also used as the primary material to prepare transparent EMI shied in a study by Jia et al. [32]. The AgNW network was formed on the sodium alginate (SA) layer by the Meyer-rod coating technique, followed by the blade coating polyurethane (PU) layer, and finally immersed in $CaCl_2$ solution to obtain a flexible calcium alginate (CA)/AgNWs/PU film. The film possessed an EMI SE of 31.3 dB, a high optical transmittance of 81 %, and impressive durability. Another flexible, transparent EMI shield based on AgNW was developed by Hu et al. [33]. Through the Meyer rod coating method, an AgNWs/polyethylene oxide (PEO) mixture was coated on a PET substrate, and then a poly(ethersulfone) (PES) layer was coated on top by a drawn-down rod coating to form a sandwiched structural PES/AgNWs/PET film. The film displayed an EMI SE of 30–40 dB in the X-band and a transmittance of ~70 %. Compared with 1D metal materials, 2D metal materials are predicted to give better EMI shielding performance ascribed to the large lateral area, which can efficiently reflect and absorb EM waves. Silver (Ag) nanoplates were erected in poly (lactic acid) (PLA) matrix through two steps: (i) coating PLA particles with Ag by electroless plating, and (ii) fusing these coated particles to form PLA/Ag nanoplate film by hot pressing [34]. The large-area Ag nanoplates in the composite resulted in excellent EMI shielding performance (60.4 dB) with a low silver content of 7.75 wt% and a thickness of 2.7 mm. Repeating reflection-absorption at the interfaces between Ag and PLA is supposed to be the mechanism of EM wave attenuation. Sambyal et al. investigated the EMI shielding performance of FeSiAl (sendust flakes)/metal hybrid materials [35]. Sendust flakes were covered by a metal layer through the electroless plating method and then incorporated with paraffin wax to form a composite. The composite based on Ni-plated sendust demonstrated a high EMI shielding performance of 65.6 dB (Fig. 2c), owing to its high electrical conductivity and good ferromagnetic properties.

Despite their high electrical conductivity, EMI shielding materials based on metals often have a heavy weight and low flexibility. The metallic coating layers would suffer from poor wear and scratch resistance and be susceptible to corrosion. The drawbacks of metal-based EMI shields hinder their broad applicability.

2.2.2. *Carbon based EMI shielding materials*

Conductive carbon materials, such as carbon black, graphite, carbon fibers, carbon nanotubes (CNT), and graphene, have been extensively studied to fabricate EMI shielding materials. The most prominent of them are CNT and graphene, which have demonstrated the ability to produce excellent EMI shielding materials with high EMI SE and good flexibility. Below, typical studies on EMI materials based on CNTs and graphene will be highlighted. The comparison of the EMI shielding performance of carbon-based EMI shielding materials is shown in Table 2.

CNT is one of the most common 1D carbon materials used to fabricate EMI shielding materials. CNT is often combined with a polymer matrix to form films. The advantage of this type of film is that it is easy to manufacture, making it suitable for large-scale production while ensuring excellent EMI shielding performance. Through facile blending methods, CNTs and polymers are mixed to obtain a uniform dispersion of CNTs in the polymer matrix. The CNT content is adjusted to increase until the composite becomes electrically conductive. In general, the EMI shielding performance of composites is directly proportional to their electrical conductivity. Wang et al. reported a poly(vinylidene fluoride) (PVDF)/multi-walled carbon nanotube (MWCNTs) composite containing 7 wt% MWCNTs that achieved an EMI SE of 30.89 dB in the X-band [36]. Li et al. mixed MWCNT and waterborne polyurethane (WPU), then fabricated a composite film using a filtration process [37]. With 10.6 wt% CNTs, the MWCNT/WPU film exhibited an EMI SE of 24.7 dB at 0.4 mm thick. Poly(ʟ-lactide) (PLLA) was used as a polymer matrix in an ultralow percolation threshold PLLA/MWCNT composite to obtain an EMI SE of 30 dB [38]. CNTs were incorporated with natural rubber (NR) in a ratio of 7:3 by filtration technique to form a strong and tough CNTs/NR film [39]. The film possessed a brilliant EMI SE of 44.7 dB with a thickness of 0.25 mm. Melt mixing followed by molding is a sequence used to prepare an EMI shield based on MWCNTs/polycarbonate (PC) composites [40], MWCNTs/polystyrene (PS) composites [41], MWCNTs/acrylonitrile butadiene styrene (ABS) [42], and MWCNTs/polypropylene random copolymer (PPCO) [43]. Meanwhile, Jia et al. used polyethylene (PE) to mix with CNT to prepare CNT/PE composite films [44]. They found that the selective distribution of CNTs at the interfaces between PE polyhedrons would enhance conductivity and EMI shielding performance. As a result, the 2.1 mm-thick CNT/PE composite film exhibited an EMI SE of 46.4 dB with a CNT content of only 5 wt%. Other than the uniform blend, a controllable blend is a strategy to construct a segregated structure of CNTs in the polymer matrixes. For these composite films, conductive networks can be formed with only a small amount of CNT composition. Kar et al. reported that the PMMA-wrapped MWCNTs localized at the interface of immiscible PVDF–ABS to construct an interconnected network of CNTs [45]. This resulted in high electrical conductivity with a CNT content of only 3 wt% and an EMI SE of 32 dB. A perfect segregated structure of MWCNTs was indicated by Ren et al. [46]. PLA_{SC} @PLLA hybrid particles were obtained by coating a poly (ʟ-lactid acid) (PLLA) with a poly (lactic acid) stereocomplex crystallite (PLA_{SC}) via a solution method before mixing with MWCNTs. Finally, through injection molding, PLA_{SC}@PLLA-MWCNT segregated film was fabricated. Wu et al. controlled temperature and pressure to make a typical semi-crystalline polypropylene (PP) during mixing with CNTs [47]. Due to the introduction of the PP solid phase, CNTs formed segregated networks in the CNT/PP composite and endowed it with an excellent EMI SE of 48.3 dB, a CNT content of 5 wt%, and a thickness of 2.2 mm. In addition, a solid-phase extrusion (SPE) method was also used to fabricate highly oriented segregated CNTs/ultrahigh-molecular-weight polyethylene (UHMWPE) composites for EMI shields [48]. Segregated structure CNTs/UHMWPUE were also obtained by mechanically mixing UHMWPE powders with CNTs and then compression-molding [49].

With 2 wt% CNTs, the composite showed a maximum EMI SE of 33.5 dB at 1 mm thickness. Liu et al. introduced a simple technique to control the segregation of MWCNTs in isotactic polypropylene/poly(ethylene-*co*-1-octene) blends (iPP/POE) [50]. The pulverization of POE particles encouraged the segregated distribution of MWCNTs in the composites, resulting in a low percolation threshold of 0.24 vol%, enabling excellent EMI shielding performance.

To further enhance the EMI shielding performance of CNT-based composites, other additives can be added to supplement their magnetic and/or electrical properties. Park's group demonstrated that EMI shielding performance increased when Ni was plated on MWCNTs in Ni-MWCNTs/high-density polyethylene composites (Ni-MWCNTs/HDPE) composite [51] and Ni-MWCNTs/epoxy composites (Ni-MWCNT/EP) composite [52]. Liu et al. reported an EMI shield made from three nanocomposite layers consisting of 15 wt% epoxy-Fe_3O_4, 5 wt% CNTs-Epoxy, and 10 wt% CNTs-Epoxy [53]. In a study published by Bhingardive et al. [54], Ni–Fe alloys were combined with MWCNTs in a poly(vinylidene fluoride) matrix. An EMI SE of 35 dB was achieved with 50 wt% of $Ni_{60}Fe_{40}$ alloy particles and 3 wt% MWCNTs. Li et al. developed a unique EMI shielding composite composed of two layers: the absorbent layer, consisting of MWCNTs and NdFeB magnetic powders as fillers in an epoxy matrix, and the reflection layer, made from MWCNT-coated non-woven fabric [55]. The absorbent layer would suppress the EM waves generated from the inside of the device, while the reflection layer could prevent the external EM waves from entering. In the research of Lei et al., Au nanoparticles were coated on the surface of CNTs to improve the electrical conductivity of Au@CNT/SA/PDMS flexible composites, leading to excellent EMI shielding performance [56]. The EMI SE reached more than 60 dB with a thickness of 2 mm and 6 wt% Au@CNT content. Yang et al. found out that the EMI SE of CNT was further densified to reduce the resistance between neighboring CNTs via thermal-induced evaporation followed by filtration processes. The densified CNT is then soaked in a gold-ion solution to fabricate CNT/Au film. The resultant film exhibited excellent EMI SE of 71 dB with a thickness of 14.3 μm in the X band, as shown in Fig. 3a [57]. By atomic precision modulation, Wu et al. reported multispectral compatible CNT films exhibiting the highest EMI SE of 78.0 dB at a film thickness of 23 μm with a high absorption effectiveness ratio of 86.9 % in the X band [58].

Graphene, with its two-dimensional (2D) structure, is known to be an effective EMI shielding material. This is feasible due to the exceptional electrical properties of graphene, which include a high electrical conductivity and a substantial number of free electrons distributed on the surface, which can interact to mitigate the energy of the incident electromagnetic waves. Furthermore, thanks to the 2D structure, the large specific surface area of graphene also increases its ability to block electromagnetic waves, as well as helping to achieve a low percolation threshold in graphene composites. In addition, the excellent thermal and mechanical properties make graphene a suitable carbon filler for EMI shielding materials. Nimbalkar et al. reported a very low percolation threshold of 0.005 vol% graphite nanoplatelets (GNP) in a polycarbonate (PC)/GNP composite [59]. The PC/GNP was prepared through facile solution mixing followed by a hot-compaction sequence. The prepared film showed an EMI SE of 35 dB with a thickness of 1 mm and 0.037 vol% GNP. To obtain excellent EMI shields, intrinsic electrical properties play a crucial role. Therefore, Zhang et al. carefully investigated the effects of the sulfonation on defects of graphene oxide (S-rLGO) to ensure the highest conductivity before mixing with P(St-BA) latex to form an EMI shielding composite via a blending-casting process [60]. A high EMI SE of 15.9 dB at a thickness of only 0.25 mm was

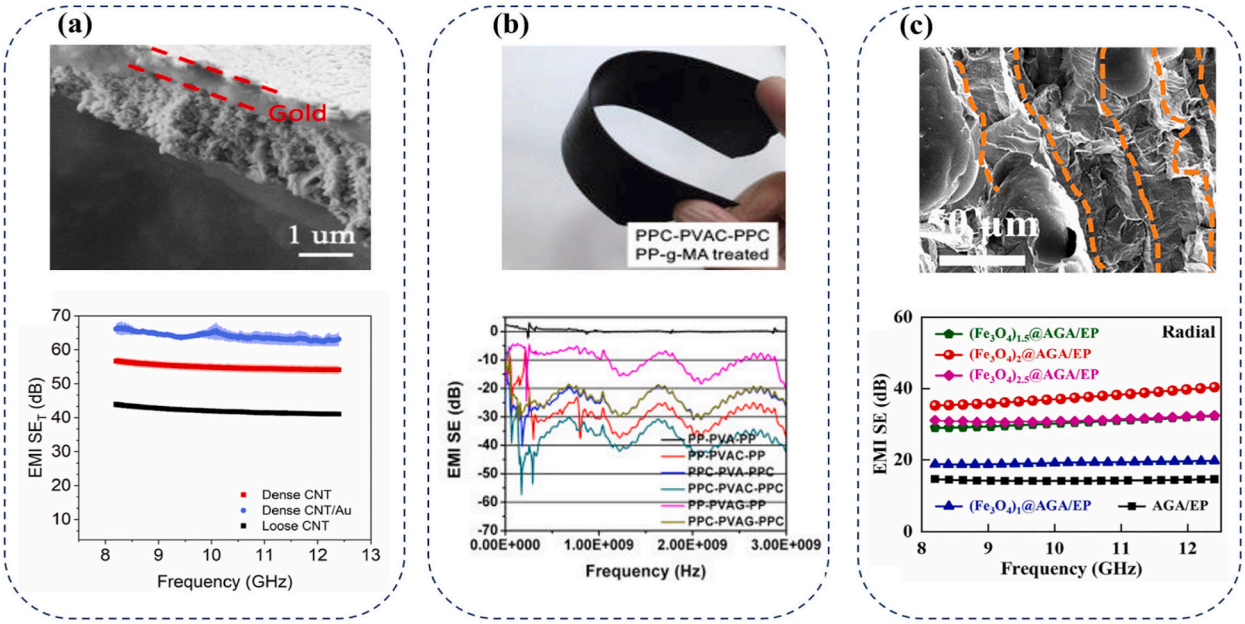

Fig. 3. Carbon-based EMI shielding materials. SEM image of the microstructure and EMI SE performance of (a) Metal-decorated densified CNT film. Reproduced with permission from Ref. [57]. Copyright 2023 Elsevier Ltd. (b) Polyvinyl alcohol/MWCNT-graphene composite. Reproduced with permission from Ref. [81]. Copyright 2015 Elsevier Ltd. (c) Fe_3O_4@anisotropic reduced graphene oxide aerogel composites. Reproduced with permission from Ref. [87]. Copyright 2022 Elsevier Ltd.

achieved. Similarly, Wei et al. prepared the mixture of P(St-BA) latex and sulfonated graphene nanosheets (S-GNS) by self-assembly via a blending method, then cast it into a composite film. The flexible P(St-BA)/S-GNS film displayed an ultrahigh EMI SE of 71.5 dB with 25 wt% S-GNS and a thickness of 1.8 mm [61]. Waterborne polyurethane (WPU) is a good choice to incorporate with graphene fillers for the fabrication of composites because it is eco-friendly, easy to form a film, and has good mechanical properties [62]. Graphene nanosheets (GN) after covalently modifying with aminoethyl methacrylate become highly compatible with a WPU matrix, leading to high electrical conductivity and EMI shielding performance of the GN/WPU composite [61]. In another approach, an electrospun WPU sheet was deposited with graphene oxide (GO) through layer-by-layer (L-b-L) assembly of two oppositely charged GO dispersions. After reducing GO into rGO, the obtained rGO/WPU composite showed a high EMI SE of 34 dB with a thickness of 1 mm [62]. George et al. reported an excellent EMI shielding composite with an EMI SE of 50 dB in the frequency range of 8–18 GHz [64]. The composite, fabricated from polypropylene (PP) and rGO by compression molding, has a thickness of 2 mm and 20 wt% rGO content. In addition, compression molding was also used to fabricate a flexible sandwich-structured silicone rubber (SR)/graphene (GN) [65]. GN content of 3 wt% was selectively localized at the surface layers of SR, leading to an EMI SE of 34.72 dB at 0.35 mm. Acrylonitrile butadiene rubber (NBR) was incorporated with GN using a conventional rubber-roll milling method to obtain a lightweight and flexible NBR/GN nanocomposite for EMI shields [66].

Graphene can be combined with another additive in a polymer matrix to enhance EMI shielding performance. The functionalized graphene oxide was decorated with silver nanoparticles to improve its electrical conductivity of 25.52 S/m with an EMI SE of 35 dB [67]. Moreover, the epoxy-based nanocomposites with reduced GO were simply mixed by centrifugation with magnetic carbonyl iron to obtain the highest EMI SE of 40 dB at 11.7 GHz [68]. On the one hand, the introduction of Ni nanoparticles has increased the performance of thermal conductivity, and EMI attenuation has gained a lot of attention. In 2015, Ni particles were decorated into the graphene via chemical and hydrogen reduction processes using nikel (II) salt solutions at the proper time and treated at the same temperatures as the polycarbonate/poly(styrene-*co*-acrylonitrile)-supported graphene/Ni-blended film with an EMI SE of 29.4 dB at 18 GHz [69] and the graphene nanoplatelet/Ni/wax nanocomposite using molecular-level mixing with an EMI SE of 40 dB in the X band [70]. Further development of employing Ni particles on graphene/polyvinylidene fluoride (PVDF)-based composites has been claimed by Liang et al. that an alternating multilayer structure of graphene sheet and Ni nanochain composite film was fabricated and highly oriented via hot compression molding and lamination. In this method, aligned nanofillers improved the in-plane thermal conductivity of composites and the multi-level EM multireflection for high performance in heat dissipation and EMI SE of 51.4 dB with a film thickness of 0.7 mm in the K_u band range [71]. Similarly, Zhao et al. reported a PVDF/carbon/Ni-based 0.6 mm-thick composite film with an EMI SE of 55.8 dB in the frequency range of 18–26.5 GHz [72]. On the other hand, magnetic iron oxide (Fe_3O_4) nanoparticles have attracted researchers to use them as an additional nanofiller in composites for enhancing EMI SE performance [73–76]. Chen et al. showed a polystyrene/Fe_3O_4/2.24 wt%-rGO hybrid material with an EMI SE of 30 dB in the 9.8–12 GHz frequency range [74]. After that, Zhan et al. demonstrated a segregated structure of flexible natural rubber/Fe_3O_4/rGO 1.6 mm-thick composite film with an EMI SE of up to 37 dB in the X band [76]. Likewise, an epoxy-based Fe_3O_4/rGO composite is well fabricated via electrostatic self-assembly and a co-prepitation approach with an EMI SE of 13.45 dB at 8.2 GHz [75]. According to the layer-by-layer technique, a multi-layered graphene nanosheet/Fe_3O_4/PVDF homogeneous composite solution was successfully prepared by ultrasonication and constructed by the casting process as a flexible film with a remarkable EMI SE of 52 dB at a thickness of 0.3 mm and high stability after bending [73]. To further upgrade the EMI SE, Yadav et al. developed a spinel ferrite nanoparticle ($NiFe_2O_4$)/rGO/elastomer nanocomposite with an EMI SE of 28.5 dB in the frequency range of 5.8–8.2 GHz [77]. The composite composed of graphene nanoplate, carbonized loofah fiber, and polyether-ether-ketone was fabricated via mechanical blending followed by hot compression and showed an EMI SE of 27.1 dB in the X band [78]. Recently, Singh et al. proved the high EMI SE of 42.83 dB in the X band of rGO/-Fe_2O_3/C/phenolic resin-based composites produced by compression molding with electrical conductivity up to 171.21 S/cm [79].

To enhance the electrically conductive network of composites, CNTs are used as a conductive bridge to connect between graphene flakes, resulting in excellent EMI shielding performance. A polycarbonate (PC)/graphene nanoplate (GNP)/multiwall carbon nanotube (MWCNT) hybrid composite was prepared by a simple melt-mixing of PC with GNP and MWCNT at 330 °C, followed by compression molding. The resultant hybrid composite showed a high EMI SE value of 21.6 dB for the hybrid with a ratio of 4 wt% (GNP/MWCNT) and an electrical conductivity of $\sim 6.84 \times 10^{-5}$ S cm^{-1} was achieved for 0.3 wt% (GNP/MWCNT) [80]. Furthermore, a low-cost, eco-friendly manufacturing method to prepare sandwich-structured composites having desirable mechanical properties, flexibility, good electrical conductivity, and EMI SE was demonstrated by Lin et al. [81] as described in Fig. 3b. The reported sandwiched structure had polypropylene/multi-walled carbon nanotubes (MWCNTs) as the surface layers, while polyvinyl alcohol (PVA)/MWCNTs and PVA/graphene nanosheets were the interlayer composites. Maleic anhydride-grafted polypropylene (PP-*g*-MA) reinforces the interfacial adhesion between the sandwich-structured composites and thereby enhances their tensile strength. The findings suggested that, with the interlayer PVA/MWCNTs, the polymer composites would have an optimal electrical conductivity of 5.8 S/cm and an EMI SE of −28.60 dB for 0.0003 GHz–1 GHz, −32.89 dB for 1 GHz–2 GHz, and −33.52 dB for 2 GHz–3 GHz bands. Similarly, interesting works based on graphene and CNT have been reported by Verma et al. that the ternary hybrid nanocomposite, which consisted of thermoplastic polyurethane as matrix and graphene nanoplatelets-carbon nanotubes hybrid (GCNT), showed a −47 dB EMI SE at the Ku-band of microwave [82]. Zhu et al. reported a cake-like flexible PDMS-coated graphene/reduced oxidized MWCNTs composite with an electrical conductivity of up to 15.15 S cm^{-1} and an EMI SE of 67.3 dB in the X-band [83]. Likewise, Jia et al. reported a 3D graphene/MWCNTs/polydimethylsiloxane composite with an EMI SE of 54.43 dB at 1400 °C [84].

Besides the electrically conductive fillers, magnetic fillers have been incorporated into composites for enhanced shielding performance, resulting in the formation of multiple filler-based EMI shielding materials. To minimize electromagnetic (EM) pollution, the intrinsic wave impedance matching and intense absorption of incoming EM radiation have been taken into consideration by polycarbonate (PC) and PVDF with doped MWCNTs and a three-dimensional crosslinked GO framework doped with ferrite nanoparticles

by Biswas et al. [85]. The unique combination of magnetodielectric couplings resulted in an EMI SE of 37 dB at 18 GHz. Moreover, an EMI SE of 57 dB was measured for a thin shield of 0.9 mm thickness of rationally stacked individual composites in a multilayer architecture [85]. Furthermore, a rapid and simple microwave method has been demonstrated to synthesize a multilayered and interconnected three-dimensional graphene-carbon nanotube-iron oxide (3D G-CNT-Fe_2O_3) hetero-nanostructure for a flexible and wideband high-performance EMI shielding film [86]. The fabricated thin and flexible composite films consist of 3D G-CNT-Fe_2O_3 nanostructures and poly(3,4-ethylenedioxythiophene) poly(4-styrenesulfonate) demonstrated excellent EMI SE over 130 dB and durability under repeated bending tests over 1000 times. Moreover, Fe_3O_4@anisotropic reduced graphene oxide aerogel (Fe_3O_4@AGA/EP) nanocomposites fabricated by one-step hydrothermal reduction reaction and unidirectional freezing reported that EMI SE reached 40.4 dB along the radial at 12.4 GHz, as shown in Fig. 3c [87]. The introduction of Fe_3O_4 nanoparticles promoted interfacial polarization among composites, leading to an improvement in shielding effectiveness. Whereas, Bera et al. demonstrated a lightweight compressible porous polydimethylsiloxane (PDMS)/FRS [ferrous ferric oxide (Fe_3O_4)], which decorated reduced graphene oxide (RGO)/single wall carbon nanohorn (SWCNH)] composite with an electrical conductivity of 2.5×10^{-2} S/cm and an EMI Se of −34.83 dB at extended Ku band [88].

2.2.3. MXenes based EMI shielding materials

Due to its metallic conductivity, higher electron density near the Fermi level, 2D structure, and excellent mechanical properties, MXene is becoming a flagship in EMI shielding materials. In 2016, the group Koo reported MXenes films ($Ti_3C_2T_x$, $Mo_2TiC_2T_x$, and $Mo_2Ti_2C_3T_x$) for EMI shielding material [4]. The $Ti_3C_2T_x$ flakes of large size were obtained from Ti_3AlC_2 MAX via a minimally intensive layer delamination (MILD) method. The large lateral-size $Ti_3C_2T_x$ flakes were laminated to form thin films by vacuum-assisted filtration. $Mo_2TiC_2T_x$ and $Mo_2Ti_2C_3T_x$ films were also prepared. The electrical conductivities of $Ti_3C_2T_x$, $Mo_2TiC_2T_x$, and $Mo_2Ti_2C_3T_x$ films achieved 4665 S cm^{-1}, 120 S cm^{-1}, and 300 S cm^{-1}, respectively. As a result, $Ti_3C_2T_x$ film showed the highest EMI SE of 48–92 dB with a thickness range of 1.5–45 μm. Especially, the EMI SE of 92 dB with a uniform thickness of only 45 μm demonstrated the highest EMI shielding performance ever known. In addition to the ultrahigh conductivity, the multilayered structure, which enhanced absorption of EM waves due to multiple reflections, and polarization losses owing to abundant functional groups on the surface of $Ti_3C_2T_x$ contributed to the excellent EMI shielding performance. Since this discovery, much more research has been conducted to develop EMI shields based on MXenes. Liu et al. treated a $Ti_3C_2T_x$ MXene film with a hydrazine solution to enhance EMI shielding performance, as presented in Fig. 4a [89]. The film thickness increased from 6 μm to 60 μm after treatment, along with the appearance of foam and widening spacing between layers in the film structure. The porous structure was formed when H_2O vapors and CO/CO_2 gases were released from the reduction reactions of hydrazine molecules with functional groups such as OH and C–OH on the surface of MXene sheets. Although a reduction in electrical conductivity from a value of 4000 S cm^{-1} (original film 6 μm) to 580 S cm^{-1} (foam 60 μm) was observed, the EMI SE value increased from 53 dB to 70 dB. The enhancement of EMI shielding performance is attributed to the multireflection of incident EM waves, leading to improved EM wave absorption due to the widening spacing between

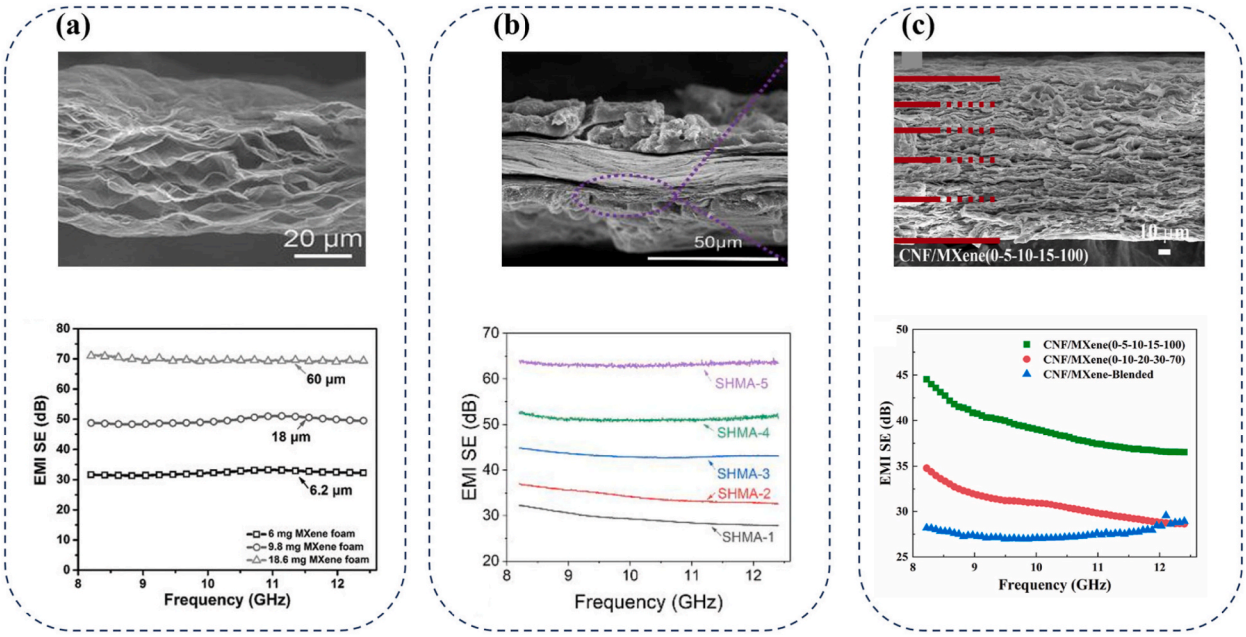

Fig. 4. MXene-based EMI shielding materials. SEM image of the microstructure and EMI SE performance of (a) MXene foam. Reproduced with permission from Ref. [89]. Copyright 2017 WILEY-VCH Verlag GmbH & Co. KGaA, Weinheim (b) MXene/aramid nanofiber composite film. Reproduced with permission from Ref. [91]. Copyright 2022 Elsevier B.V. (c) $Ti_3C_2T_x$/CNF composite film. Reproduced with permission from Ref. [92]. Copyright 2022 Elsevier Ltd.

MXene layers in the porous structure. The treatment also resulted in the hydrophobic properties and good oxidation stability of the MXene foam. In addition, the group Koo continued reporting another member of the MXene family, Ti_3CNT_x, as an outstanding EMI shielding material [90]. Ti_3CNT_x nanosheets, which were prepared by etching from their corresponding MAX phase Ti_3AlCN, were laminated into a 40-μm-thick film through vacuum filtration. The film possessed an electrical conductivity of 1125 S cm^{-1} and an EMI SE of 61 dB. Interestingly, the structure of the Ti_3CNT_x film also transformed from compact to porous under annealing treatment. Annealing temperature was up to 350 °C, and the porosity was proportional to temperature. The effect of annealing temperature on the electrical conductivity of the film was observed with an enhanced electrical conductivity of 2475 S cm^{-1} at 250 °C. It was ascribed to the removal of adsorbed H_2O molecules and surface terminations. Further increasing the annealing temperature to 350 °C, the surface oxidation of Ti_3CNT_x occurred, resulting in a slight decrease in electrical conductivity. However, the EMI SE of the film still increased and achieved 116 dB, which is higher than the EMI SE of annealed $Ti_3C_2T_x$ film (93 dB) with the same thickness. This outstanding EMI shielding performance was contributed by the induced porous material and improved electrical conductivity.

The hydrophilicity of MXenes endows them with the ability to easily form stable dispersions and combine with polymer matrix into low-percolation threshold composites. Therefore, EMI shielding materials developed from MXenes polymer composites are attracting more and more attention. Luo et al. incorporated $Ti_3C_2T_x$ MXene into natural rubber (NR) to form an EMI shielding film with a thickness of 251 μm [93]. A mixture of $Ti_3C_2T_x$ colloidal and NR latex with 6.71 vol% $Ti_3C_2T_x$ was vacuum-filtrated on filter paper. After peeling, the $Ti_3C_2T_x$/NR film was dried entirely at room temperature. The film exhibited an excellent electrical conductivity of 1400 Sm^{-1} and an EMI SE of 53.6 dB. Owing to the combination between MXene and NR, the mechanical properties of the film were enhanced, with tensile strength and modulus increasing by 700 % and 15000 %, respectively, as compared to those of neat NR.

The vacuum-assisted filtration method was also used to fabricate an ultrathin EMI shielding based on $Ti_3C_2T_x$ MXene and aramid nanofiber (ANF) [94]. The ANF/MXene with a weight ratio of 20:80 showed an excellent conductivity of 879.0 S/cm, resulting in an EMI SE of 40.6 dB with a thickness of only 3.2 μm. Similarly, Liu et al. mixed chitosan (CS) solution with $Ti_3C_2T_x$ MXene dispersion, then filtered by vacuum-assisted filtration to collect a film [95]. The CS/MXene film displayed an EMI SE of 34.47 dB with a thickness of only 37 μm and a $T_3C_2T_x$ content of 75 %. The strong, light, and durable composites of MXene integrated with ANF were successfully fabricated in the form of anisotropic aerogel [96] and film [91] with excellent EMI SE. Yao et al. investigated the EMI SE performance of a hierarchical structure superhydrophobic MXene/aramid nanofiber (SHMA) film (Fig. 4b) prepared by the layer-by-layer method and hot-pressing [91] at temperatures ranging from 25 to 300 °C. The superhydrophobic MXene/ANF film showed a high EMI SE of 63.2 dB at a thickness of 70 μm. Meanwhile, Wang et al. claimed that the conductive composite film of AgNW/MXene/polyurethane exhibited an EMI SE of 27.1 dB with a high transmittance of 82.8 % [97]. The polyvinylidene fluoride (PVDF)-MXene composite nanofiber, which is decorated by ZnO, was developed as a flexible and stable film with an EMI SE of 61 dB [98]. Due to the 2D structure of the MXene nanosheet, MXene/polymer nanocomposite films fabricated by vacuum filtration often possess a nacre-like ‘‘brick and mortar’’ with a highly ordered nanostructure of MXene [99–101]. Liu et al. reported a nacre mimetic polyurethane (PU)/$Ti_3C_2T_x$ MXene composite film for EMI shielding [99]. The composite film showed an ultrahigh electrical conductivity of ~2897.4 S cm^{-1} and excellent EMI SE of 27.6 dB in the X-band with an ultra-small thickness (<10 μm) and 80 wt% $Ti_3C_2T_x$. In addition, PU/$Ti_3C_2T_x$ displayed flexibility and good mechanical properties, with a tensile strength of ~100 MPa and a fracture toughness of ~3.0 MJ m^{-3}. Numerous techniques have been proposed to enhance the EMI SE performance of composite materials composed of $Ti_3C_2T_x$/cellulose nanofiber (CNF), including a gradient structure [92], an aligned structure [102], a layered structure [103], a porous structure [104], and a 3D printed structure [105]. Ma et al. proved that the MXene and CNF are well-constructed together to maximize the EMI SE of composites by controlling the conductive gradient layer via layer-by-layer vacuum filtration [92], as shown in Fig. 4c. The best EMI SE of CNF/MXene (0-5-10-15-100) composites performed an EMI SE of 44.5 dB at 105 μm in the X band. The nacre-like lamellar structure of $Ti_3C_2T_x$/CNF composite paper was prepared by Cao et al. through a vacuum-filtration-induced self-assembly process [101]. This

Table 3
Comparison of EMI shielding performance of MXene-based EMI shielding materials.

Material	Filler content (wt%)	Thickness (mm)	Frequency (GHz)	SE_T (dB)	Ref.
$Ti_3C_2T_x$	100	0.045	8.2–12.4	92	[4]
$Ti_3C_2T_x$ foam	100	0.06	8.2–12.4	70	[89]
Ti_3CNT_x	100	0.04	8.2–12.4	116	[90]
$Ti_3C_2T_x$/NR	6.71	0.251	8.2–12.4	53.6	[93]
$Ti_3C_2T_x$/ANF	80	0.0032	8.2–12.4	40.6	[94]
$Ti_3C_2T_x$/CS	75	0.037	8.2–12.4	34.7	[95]
$Ti_3C_2T_x$/ANF aerogel	80	2.5	8.2–12.4	65.5	[96]
$Ti_3C_2T_x$/ANF film	80	0.07	8.2–12.4	63.2	[91]
AgNW/MXene/PU	–	–	8.2–12.4	27.1	[97]
(PVDF)-MXene ZnO	10	0.015	8.2–12.4	61	[98]
$Ti_3C_2T_x$/PU	80	0.01	8.2–12.4	27.6	[99]
$Ti_3C_2T_x$/PEDOT:PSS	87.5	0.0111	8.2–12.4	42.1	[100]
$Ti_3C_2T_x$/CNF	80	0.074	8.2–12.4	25.8	[101]
$Ti_3C_2T_x$/CNF	26	0.105	8.2	44.5	[92]
Delaminated-MXene/CNF	–	0.02	8.2–12.4	36.51	[102]
Layered-MXene/CNF	–	0.0101	8.2–12.4	44.6	[103]
CNF/MXene-50/MCHSM-5	50	0.05	8.2–12.4	41.7	[104]
m-$Ti_3C_2T_x$)/CNFs	90	3.3	8.2–40	80.3	[105]
$Ti_3C_2T_x$/Epoxy	15	2	8.2–12.4	41	[106]

structure not only possesses strengthening, toughening with tensile strength (135.4 MPa), fracture strain (16.7 %), and folding endurance (14260 times), but also electrical conductivity (739.4 S m^{-1}). As a result, the paper achieved an EMI SE of 25.8 dB with a thickness of 74 μm. In the "brick-and-mortar" structure of film reported by Liu et al., poly(3,4-ethylenedioxythiophene)−poly(styrenesulfonate) (PEDOT:PSS) served as the "motar," while $Ti_3C_2T_x$ nanosheets assumed the role of "bricks" [100]. As known as an intrinsic conductive polymer, the presence of PEDOT:PSS led to excellent electrical conductivity (340.5 S/cm) of the film, resulting in a superior EMI SE of 42.10 dB with a thickness of only 11.1 μm. Furthermore, the mechanical properties of the film were significantly improved, with a tensile strength of 13.71 MPa and a fracture strain of 0.29 %. For a scalable and facile fabrication method, Wang et al.

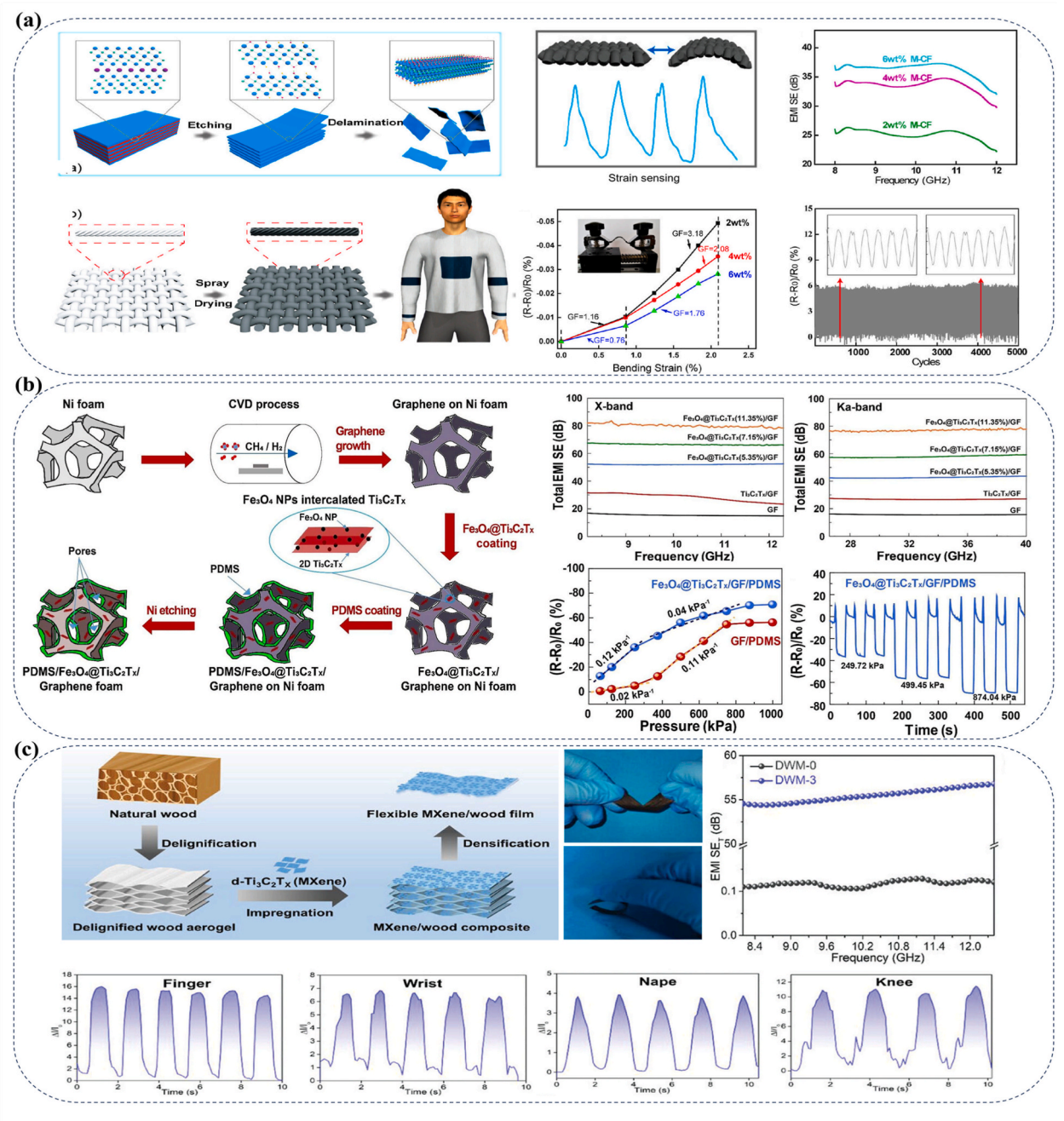

Fig. 5. Preparation procedures and characterization of EMI shielding materials with strain sensing functions (a) MXene-decorated cotton fabric. Reproduced with permission from Ref. [9]. Copyright 2020 American Chemical Society. (b) Fe_3O_4@$Ti_3C_2T_X$/GF/PDMS composite. Reproduced with permission from Ref. [114]. Copyright 2020 Elsevier B.V. (c) MXene functionalized wood composite film. Reproduced with permission from Ref. [115]. Copyright 2023 Wiley-VCH GmbH.

used a mechanical mixing process to obtain a mixtrure of annealed $Ti_3C_2T_x$ and epoxy, which was then poured into a mold to form a $Ti_3C_2T_x$/epoxy nanocomposite [106]. The composite exhibited an electrical conductivity of 105 S/m and an EMI SE of 41 dB with a $Ti_3C_2T_x$ content of 15 wt% and a thickness of 2 mm. Table 3 summarizes the EMI shielding performance of MXene-based EMI shielding materials.

3. Beyond EMI shielding function

3.1. Strain sensing function

Strain sensing materials have great potential in today's critical and innovative applications, such as robotics and wearable electronics, as they can assist robotic systems to sense tactile feedback or collect signals for monitoring the health of wearers. For strain sensor materials, their accuracy is one of the most important requirements. However, they are very susceptible to electromagnetic interference from external sources or caused by internal components. In addition, the trend toward multifunctionalities, performance improvement, and size reduction in electronic devices has encouraged research on multifunctional materials. Therefore, the introduction of multifunctional EMI shielding materials with strain sensing ability is necessary to substitute for a typical sensing material in the device without any additional EMI protection. These multifunctional EMI shielding materials can protect the equipment, the human body, or the robotic systems from harmful EM waves and EMI while providing strain sensing ability.

To the best of our knowledge, the strain sensing function in multifunctional EMI shielding materials is mainly based on resistive-type strain sensing. These materials are generally fabricated by depositing thin conductive layers onto stretchable substrate surfaces or embedding conductive nanomaterials into elastomers. Therefore, multifunctional EMI shielding materials with strain sensing ability can be classified based on supporting materials.

To meet the increasing demand for wearable devices, textiles have been used as supporting materials with the advantages of flexibility, stretchability, ventilation, ambient stability, and even washability. They have been developed to make sensors [107], energy storage materials [108], electrodes [109], and EMI shielding materials [110]. So far, large-area fabrication of multifunctional EMI materials with strain sensing capabilities that are textile-based has been achieved [111,112]. Conductive materials, such as metallic nanomaterials, conductive polymers, carbon nanomaterials, and MXenes, can be used to coat the surface of fabrics to form multifunctional EMI shielding fabrics. Nevertheless, it still has several drawbacks caused by the low electrical conductivity, weak interfacial adhesion, and unsatisfactory mechanical properties of the stretchable substrate, such as the low EMI SE, low sensitivity (i.e., gauge factor), durability, response speed, stability, and resilience [113].

Zhang et al. reported a MXene-decorated cotton fabric (M − CF) for a multifunctional EMI shielding textile with strain sensing ability to recognize human motion [9], as shown in Fig. 5a. $Ti_3C_2T_x$ MXene ink was prepared by etching Ti_3AlC_2 with a hydrochloric acid (HCl) and lithium fluoride (LiF) mixture, followed by the delamination process. Via adjusting spray coating-drying cycles, the MXene nanosheets were loaded on a templated cotton fabric, resulting in a conductive surface. Owing to the excellent electrical conductivity of MXene, the M − CF performed a high average EMI SE of 0.33 mm thickness, which was about 25, 33, and 36 dB, corresponding to 2, 4, and 6 wt% MXene loading content, respectively, in the X-band. Besides the main function of EMI shielding, the M − CF also had superior sensitivity to bending strain. The strain-bending sensing property was due to the changing conductive path inside the fabrics. Under bending, the adjacent MXene nanosheets were distanced, and the relative resistance changed versus the bending strain of MXene-modified fabrics. The gauge factor (GF), which represents the sensitivity, can be calculated by the slope of relative resistance change-bending strain curves. The 2 wt% MXene loading content M − CF sensor showed the highest GF compared with the other two sensors due to the maximum change in resistance with the same bending strain. Furthermore, the sensing performance showed high stability and durability under cyclic bending of 5000 cycles. Due to their outstanding flexibility, high sensitivity, and stability, M–CF–based sensors have broad application prospects in wearable devices to track human movements, such as finger flexion, hand motion, heart rate detection, and pronunciation recognition.

Sang et al. fabricated a multifunctional EMI shielding textile by dip-drying a non-woven fabric using silver nanowires (AgNWs) dispersion and multiwall carbon nanotubes (MWCNTs) dispersion, respectively, followed by solution-casting with poly(vinylidene fluoride) (PVDF) solution [116]. This EMI shielding textile possessed an EMI SE of 34 dB with a thickness of 390 μm and demonstrates its multifunctional ability through a force-sensing (0, 20, 44, and 60 N) property due to piezoelectric phenomena that can detect human body movements, such as jumping, running, finger joint bending, and heart beating with self-power. A self-powered strain sensor based on piezoelectric and triboelectric phenomena was also developed by Zhang et al. [117]. The sensor was composed of several small-sized layers of Ag thin films deposited on both sides of a polarized PVDF film attached to a large-sized layer of Ag-coated fabric sandwiched between two rubber layers. It exhibited a good strain-sensing performance with a strain of 40 % that would monitor the breathing process. In addition, the material shielded more than 99.9978 % of EM waves ranging from 0 to 1.5 GHz. Through dip-coating reduced graphene oxide and spray-coating $Ti_3C_2T_x$ MXene, Zheng et al. have successfully fabricated rGO/MXene-decorated cotton fabric (RMC), a smart cloth with many functions [118]. With a thickness of ~500 μm, the RMC provided an EMI SE of 29.04 dB. Another interesting function of this fabric is its bending-strain sensing ability with negative resistance variation and high sensitivity to monitor human motions, including bending fingers, elbows, knees, and swallowing. The negative resistance variation phenomenon has also been recorded by Zhang et al. when they tested stretching-strain sensing of a flexible Ni@PET-g--PAO/Fe_3O_4 textile, which was fabricated by radiation-induced graft polymerization (RIGP) treatments and electroless plating [118,119]. The strain sensor showed that the performance of a fast and repeatable response displayed long-term stability in the strain range of 0–40 % and an EMI SE of 19.4 dB at an operating frequency of 0.05–1 Hz.

Besides fabric-based shielding, multifunctional EMI shielding with strain sensing ability can be fabricated based on elastomer

composites. Nguyen et al. proposed a multifunctional EMI shielding skin with the dual purpose of protecting robotic systems from EM waves and sensing pressures, mimicking the functions of human skin [114]. The EMI shielding skin was a Fe_3O_4@$Ti_3C_2T_x$/GF/PDMS composite, as shown in Fig. 5b. A graphene foam (GF) synthesized by CVD was decorated by Fe_3O_4 nanoparticles that intercalated the $Ti_3C_2T_x$ nanosheets, followed by reinforcement in polydimethylsiloxane (PDMS) matrix. The Fe_3O_4@$Ti_3C_2T_x$/GF/PDMS composite exhibited an ultrahigh EMI SE of 80 dB in 8.2–12.4 GHz and 77 dB in 26.5–40 GHz with 11.35 wt% filler content and a thickness of 1 mm due to excellent absorption SE. Furthermore, due to their good elasticity, rapid recovery, highly conductive nature, and large specific surface area, the deformation of Fe_3O_4@$Ti_3C_2T_x$/GF/PDMS composites resulted in a change in electrical resistance, leading to a promising pressure-strain sensing performance under the external pressure range of 62.4–700 kPa. The time-dependent $(R - R_0)/R_0$ of Fe_3O_4@$Ti_3C_2T_X$/GF/PDMS under different press releases are shown. When pressurization, the conductive pathways were generated from contact of graphene-graphene, $Ti_3C_2T_x$-$Ti_3C_2T_x$, and graphene-$Ti_3C_2T_x$, thereby the $(R - R_0)/R_0$ of the composites became negative and proportional to the applied pressure. When released, the resistance recovered to its original status; thus, $(R - R_0)/R_0$ became zero. This result opens the possibility of being used as a multifunctional EMI shield for wearable electronics and robotics.

Liang et al. reported a sponge of polyurethane@polydopamine@silver nanoparticles (PU@PDA@Ag), fabricated by a facile bio-response method consisting of two steps: decorating PDA on the surface of the PU sponge and in-situ growing Ag nanoparticles on the PU@PDA [120]. Due to its excellent compressibility, the sponge possesses a human motion-sensing ability, such as walking, bending knees, fingers, wrists, and elbows, with a maximum of 80 % compression strain. The compression reduced the gap between Ag nanoparticles, improved the conductive network, and reduced electrical resistance, which quickly responded to the deformation of the sponge. Besides, the PU@PDA@Ag sponge exhibited an impressive EMI SE of 84 dB with a thickness of 5 mm. Silver nanoparticles (AgNPs) were used by Wu et al. in another report, which showed a 14.8 μm-thick coating film with an EMI SE of 37.8 dB [121]. The coating material was a mixture of AgNPs and polystyrene-*block*-poly(ethylene-*co*-butylene)-*block*-polystyrene (SEBS) that would be applied to various substrates to demonstrate multifunctionality. SEBS/AgNPs were coated on an elastic tape to form a strain sensor that exhibited excellent sensitivity (66 and 1075 in the strain range of 0–51 % and 53–60 %, respectively) and fast response time (approximately 100 ms). By a scalable technique of melt blending and compression molding, Zhao et al. fabricated a flexible poly (ether-*block*-amide) (PEBAX)/graphene composite film, which performed an average EMI SE of 30.7 dB with a thickness of 2 mm and only 8.91 vol% graphene content [119]. In addition, the film exhibited a negative pressure coefficient (NPC) effect of resistance with increasing outer pressure. The compression molding technique was also used by Yuan et al. to fabricate a 1.8-mm film composed of branched carbon nanotubes (CNS) and recycled epoxy [122]. The CNS formed a segregated structure in composite as an electrically conductive network, leading to good strain-sensing performance and EMI shielding performance (EMI SE of 22 dB) with a CNS content of only 1 wt%. Based on the natural wood structure, the MXene nanosheets are impregnated onto the delignified wood, followed by a densification process to prepare a flexible MXene/wood film with high EMI SE performance, as shown in Fig. 5c [115]. The advantage of this method is that well-aligned celluloses support the arrangement and stacking of MXene on the cellulose framework, resulting in a highly conductive, flexible, and robust MXene/wood composite. This composite reached 55.5 dB with a MXene content of 32.5 wt% in the X band. In addition, the MXene functionalized wood composite film showed a high sensitivity to human motions (finger, wrist, nape, and knee).

Jia et al. reported sandwich-like structure graphene oxide/silver nanowire (GO/Ag-*x*L, *x* represents the number of layers) films, which are fabricated through vacuum-assisted self-assembly [123]. The GO/Ag-7L displayed a maximum EMI SE of 62 dB with a thickness of 8 μm in the broad-band frequency range of 8–40 GHz and acted as a bending strain sensor with high sensitivity and quick response. Therefore, it could be applied to protect EMI and detect motions in robotic systems. Also targeting robotic applications, Pu et al. developed a multifunctional electronic skin (M-E-skin) [124]. The M-E skin consisted of AgNW spray-coated onto the rough PDMS and another layer of AgNW deposited on the smooth PDMS. These components came together to create an exceptional pressure sensor characterized by high sensitivity (9.8×104 kPa^{-1} for the pressure range 0–0.2 kPa and 3.5×103 kPa^{-1} within 0.2–20 kPa), broad operating range (0–20 kPa), rapid response and relaxation times (<62.5 ms), excellent pressuring-relaxing stability (10 kPa, 1000 cycles), low operating voltage (0.1 V), low power consumption (1.5 nW), and low detection limit (5 Pa). It also possessed EMI shielding performance, with shielding effectiveness greater than 99.66 %.

3.2. Humidity sensing function

The rapid development of flexible and wearable EMI shielding materials has driven the scavenging of their combined functionality with humidity or human skin moisture monitoring. The humidity sensing functionality of the EMI shielding textiles, which are widely required as electromagnetic protection clothes for pregnant women, military, and electronics industry workers can be useful to monitor vital physiological signals from sweat, skin moisture, and breath in real-time. The noninvasive real-time monitoring of human physiological biomarkers, such as humidity levels in the skin, can yield crucial information about the metabolic and aging states and healing progress of wounds [125,126]. Moreover, humidity sensors can detect sweat rates from different regions of the body to enable real-time monitoring of vital information on health conditions, such as hypohydration (dehydration) or hyperhydration, and other diseases [127,128], or non-invasively monitor the sweat rate from a different region of the human body (wrist, neck, or forehead) after exercise [129]. The MoS_2-based humidity sensors could effectively detect sweat from 3 mm of distance from the skin by decreasing the electrical resistance according to the water content in the sweat from different regions of the body.

Compared to hydrophobic MoS_2 and graphene, the widely studied EMI shielding material 2D MXene could be more suitable as a humidity sensor thanks to its hydrophilic surface and metallic conductivity [130]. Furthermore, $Ti_3C_2T_x$ MXene had a multilayer nanostructure with hydration/dehydration behavior on water molecules and showed hydration heterogeneity over a wide range of relative humidity (RH) [131,132]. The interlayer spacing between MXene was affected by this hydration or dehydration of water

molecules, causing changes in electrical conductivity. Indeed, it was demonstrated by An et al. in a comprehensive study on the humidity sensing mechanism of the $Ti_3C_2T_x$/PDAC (MXene/polyelectrolyte) multilayer films prepared by layer-by-layer assembly [133]. The MXene interlayer distance increased at high humidity, leading to an increase in tunneling resistance. Conversely, at low humidity, the interlayer distance decreased, resulting in the recovery of resistance. This sensing mechanism was supported by the quartz crystal microbalance and ellipsometry measurements by observing the film thickness upon humidity variation. Therefore, the MXene-based wearable material offers a practical solution by combining humidity sensing for health monitoring with EMI shielding materials.

It is imperative to develop an efficient strategy for permeable, porous, nontoxic functional wearable shielding materials or fabrics for the comfort and safety of military personnel, pregnant women, industrial workers, etc. Various methods have been proposed to address this problem, including the biodegradable, non-toxic, and renewable biomass polymer chitosan/MXene (CS/$Ti_3C_2T_X$) film-based EMI shielding material with humidity sensing reported by Lu et al. [95]. Three different concentrations of MXene solution were uniformly dispersed into a certain volume of CS solution, and the mixture was filtered by a sand core funnel connected with a vacuum pump to obtain CS/MXene films with different MXene contents. The well-aligned MXene layers with 75 % concentration yielded CS/MX-75 films of 37-μm thickness with a high electrical conductivity of 1402 ± 70 Sm^{-1}, resulting in a high EMI shielding effectiveness of 34.7 ± 0.2 dB in the X-band frequency (8.2–12.4 GHz). Furthermore, the relative change of resistance ($\Delta R/R_0$) in the CS/MX-75 film remarkably increased as humidity exposure time increased in high relative humidity (RH) of 73 % and could be used to identify deep and normal breathing by monitoring the trace amounts of moisture from exhaled air.

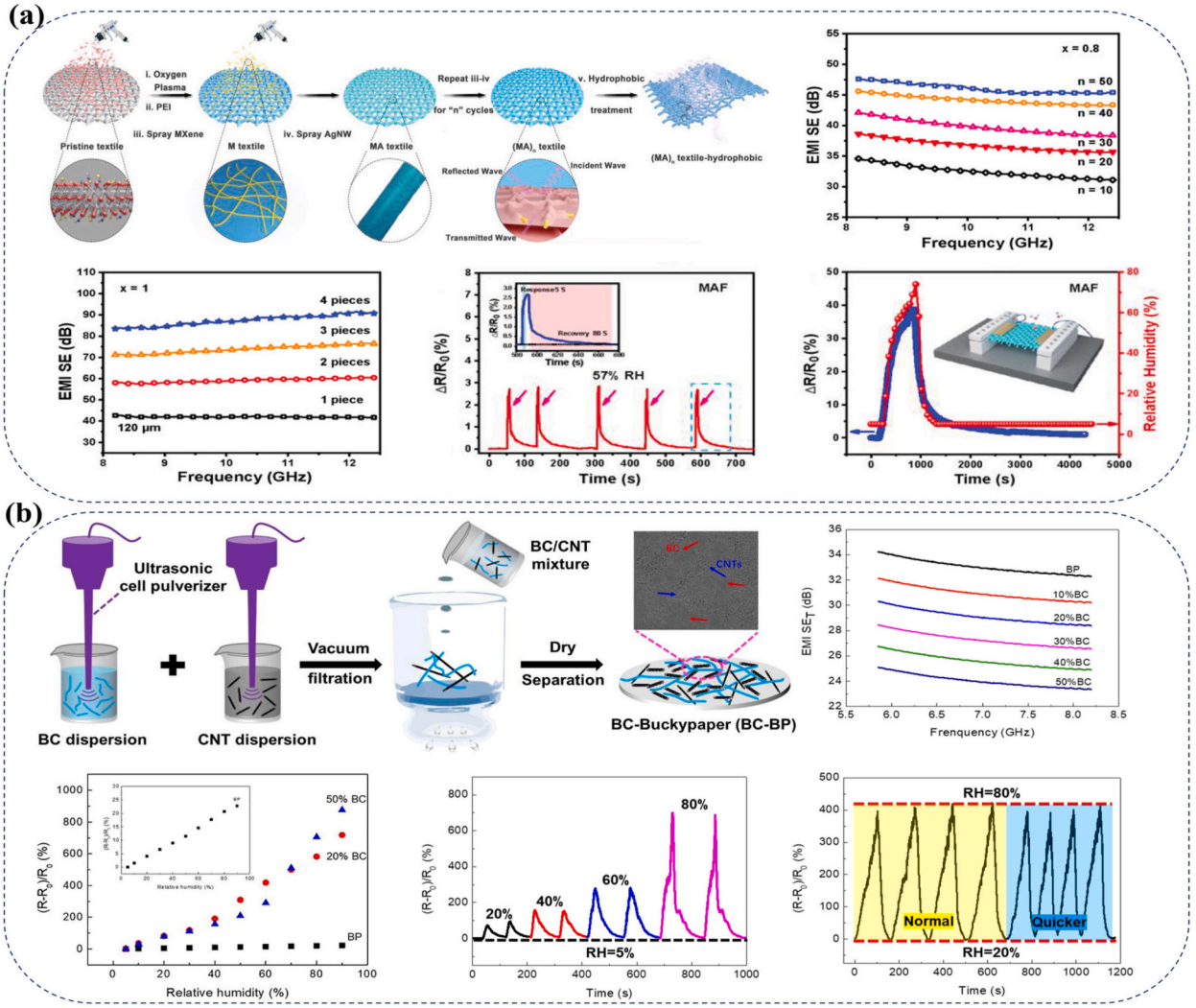

Fig. 6. Preparation procedures and characterization of EMI shielding materials with humidity sensing functions (a) Flexible and multifunctional silk textiles with biomimetic leaf-like MXene/Silver nanowire nanostructures. Reproduced with permission from Ref. [134]. Copyright 2019 WILEY-VCH Verlag GmbH & Co. KGaA, Weinheim. (b) Bacterial cellulose-reinforced carbon nanotube buckypaper. Reproduced with permission from Ref. [135]. Copyright 2022 Elsevier B.V.

Fig. 6a illustrates a vacuum-assisted layer-by-layer (LbL) assembly approach for fabricating superhydrophobic silk textiles for EMI shielding and humidity monitoring applications. $Ti_3C_2T_x$ MXene and silver nanowire (AgNW)-decorated silk fabrics $(MA_x)_n$ were prepared by vacuum-assisted LbL spray coating in repeated cycles, where M is MXene, A is AgNW, x is the concentration of AgNW, and n is the number of spray cycles [134]. The AgNWs and MXene nanosheets are incorporated into porous textiles to generate a highly conductive leaf-like nanostructure, leading to high electrical conductivity, EMI shielding, and humidity sensing responses. The leaf-like nanostructure consisted of $Ti_3C_2T_x$ as the conductive lamina and AgNWs as the conductive veins. Note that the electrical conductivity increased linearly with an increase in AgNW concentration; on the contrary, the higher concentration resulted in a continuous film that reduced the air permeability of the multifunctional textile. The EMI shielding efficiency increased linearly with an increasing number of cycles and AgNWs content over the X-band frequency range. Interestingly, the 120 μm-thick leaf-like structure of $(MA_1)_{10}$ silk showed an EMI SE of 42 dB, which was increased up to 90 dB by adding four layers of leak-like silk throughout the X-band. The MAF silk showed consistent resistance changes under the repeated exposure of RH 57 % testing, indicating stable and durable humidity sensing with a response and recovery time of 5 s and 80 s, respectively, which is comparable to a commercial humidity sensor. Therefore, MXene-based multifunctional textiles or composites, with excellent humidity sensing capabilities, hold promise as smart wearable garments for human health monitoring and EMI shielding applications.

Fan et al. demonstrated that a bacterial cellulose (BC)-supported carbon nanotubes (CNT) buckypaper exhibited high humidity sensing properties in the wide relative humidity range (5–90 %RH) and good EMI SE performance, as shown in Fig. 6b [135]. The buckypaper was fabricated using vacuum filtration of BC and CNT mixtures following drying. The EMI SE of composites decreased with the increase in BC content due to the reduction in electrical conductivity. The highest EMI SE was as high as 33.04 dB in the frequency range of 5.85–8.2 GHz (C-band). The relative resistance of composites changed as a function of RH from 5 to 90 % for different BC contents. The 50 %BC buckypaper-based humidity sensor showed a dynamic response with high stability when humidity varied between 5 % and 20, 40, 60, and 80 %RH. Jang et al. combined multi-walled carbon nanotubes with graphene nanoplatelets via powder mixing and hot press to produce a composite with a high EMI SE of 50 dB at 40 vol% MWCNT and a humidity sensitivity of 82.22 %

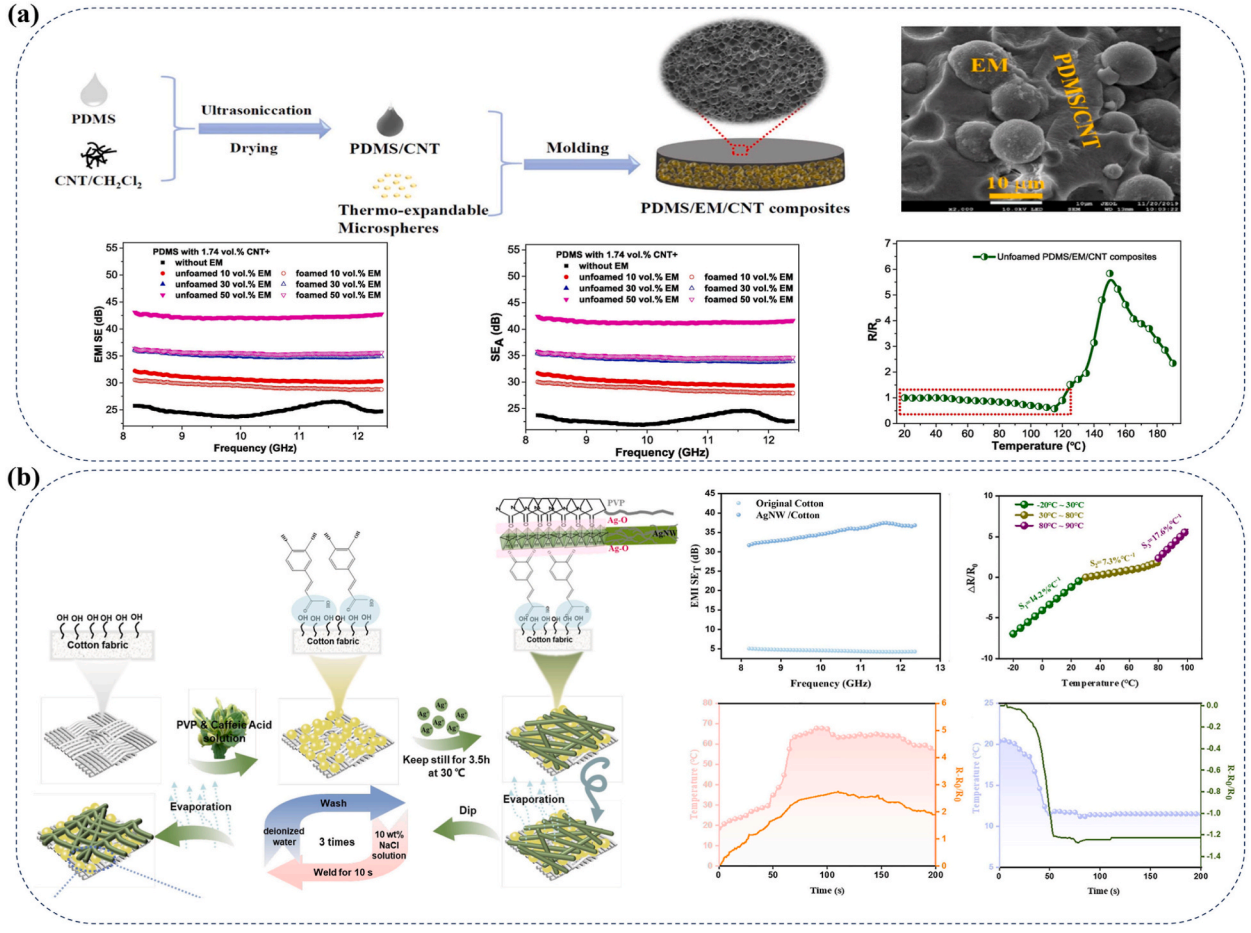

Fig. 7. Preparation procedures and characterization of EMI shielding materials with temperature sensing function (a) polydimethylsiloxane/multi-walled carbon nanotube/thermo-expandable microsphere foam composite. Reproduced with permission from Ref. [139]. Copyright 2020 Elsevier B. V. (b) Silver nanowire/cotton fabric composite. Reproduced with permission from Ref. [140]. Copyright 2023 Elsevier B.V.

[136].

3.3. Temperature sensing function

The demand to develop EMI shielding materials with temperature sensing functions has also been increasing due to their ability to sense temperature for applications in temperature control and warning systems, which protect electronic devices and circuits from operating in severe conditions precisely and speedily, such as outdoors and automatic continuous operation. The temperature sensing function is integrated into EMI shielding materials by blending the proper materials into a composite structure that is sensitive to temperature. When the temperature increases, the conductivity of the composite material increases (positive temperature coefficient (PTC) effect) or decreases (negative temperature coefficient (NTC) effect). This change in conductivity is caused by the thermal expansion of the matrix (polymer) phase at elevated temperatures.

In 2005, Farid El-Tantawy demonstrated functional conducting elastomer blends with temperature sensing and EMI shielding abilities based on the combination of butyl rubber (IIR), polyethylene (PE), and other additives [137]. The network structure and electrical conductivity of elastomer blends on PE loading were investigated. The blends with a PE content of 10 wt% showed high sensitivity to temperature and high EMI shielding up to 61 dB in the frequency range of 1–16 GHz. Similarly, a few years later, El-Tantawy and his colleagues published a work on natural rubber (NR), PE, and Bi-based superconductor (BSCCO) nanoparticles as the main components of conducting elastomer blends for high-sensitivity temperature sensors and EMI shielding materials [138]. The composites behaved as both NTC and PTC effects at a certain temperature (called double thermistors' effect) through the conduction mechanism of tunneling (activation) and surface acceptor state (hopping energies) in the blends. In addition, the NR composite with 10 wt% PE performed with a shielding effectiveness of 44–60 dB at the microwave frequency (8–12 GHz). Liu et al. proposed the segregated polypropylene/cross-linked poly(ethylene-*co*-1-octene)/multi-walled carbon nanotube nanocomposites [50], which were sensitive to a wide temperature range of 45–120 °C and 150–190 °C with the NTC effect. However, the EMI SE of this composite structure with 3.0 vol% MWCNTs (thickness 1.2 mm) was only as low as 25 dB.

Recently, scientists from Southwest University, China, have successfully developed a foam-structured composite material by introducing the thermo-expandable microsphere (EM) into polydimethylsiloxane (PDMS) and multi-walled carbon nanotubes (CNT) with excellent temperature sensing and high EMI shielding performance [139]. Fig. 7a shows the fabrication process of the composite with the uniform distribution of EM into the PDMS/CNT matrix and its EMI SE and sensing performances. The PDMS/EM/CNT composite performed firstly the NTC effect, then changed into the PTC effect from near the T_g point (108 °C) of the thermoplastic microsphere, and finally came back to the NTC behavior at 150 °C. These temperature responses of composites through three heating processes could be explained by the high crosslinking density of PDMS at the first stage; the thermal expansion of EM, which destroyed partly the original conductive paths with the enlarged distance between adjacent CNT fillers, resulting in high temperature sensitivity at the second stage; and the failure of the microsphere and reconstruction of CNT filler-conductive paths at the final stage. The unfoamed composite with 50 vol% EM showed a high EMI shielding performance of 43 dB in the X-band with an absorption-dominant mechanism.

Besides, the temperature-sensing properties with EMI SE performance were investigated early in the functional textile materials. The AgNWs/MXene-based knitted fabric prepared by dip-coating showed an EMI SE of 44 dB in the frequency range of less than 3 GHz [141]. The composite exhibited a temperature coefficient of resistance of −0.07 %/°C under the NTC effect in the temperature range of 25∼126 °C. On another cotton fabric, Zing et al. fabricated a flexible silver nanowire/cotton fabric that was highly sensitive to temperature by using agents including caffeic acid and polyvinypyrrolidone at room temperature, as shown in Fig. 7b [140]. The composite showed a good EMI SE of 38.2 dB in the X band with a thickness of 0.225 mm. Meanwhile, the relative resistance of composite fabric increased with increasing temperature at −20∼90 °C. The high sensitivity of AgNW-coated cotton to temperature was clearly observed in both increasing temperatures from 18 °C to 68 °C and falling temperatures from 22 °C to 12 °C, corresponding to the increase and the decrease in their relative resistances.

3.4. Heating function

Under low ambient temperatures, such as in icy regions, polar regions, or outer space, electronic devices also become numb to inactivity. Batteries, displays, sensors, touch screens, etc. Components of electronic devices will stop working in extreme cold. The materials for the devices can even crack, and EMI shielding components are no exception. To minimize the harmful effects of cold environments, the devices are equipped with heating elements. Therefore, the idea of combining the EMI shielding function with the heating function in one material has attracted a lot of attention because these two functions are basically based on the good electrical conductivity of the material. By endowing heating capability, the multifunctional EMI shielding materials will be able to withstand the extreme cold ambient temperature conditions, assisting to reduce distortion, frost formation, and surface freezing, as well as ensuring normal operation for the device. Moreover, if these multifunctional EMI shields with heating abilities are used in wearable electronic devices, they can help keep the wearer warm and protect their health while providing a comfortable feeling.

Most electromagnetic wave shielding materials are based on excellent electrically conductive properties [56], which benefit the Joule heating effect. An electric-to-heat conversion is based on Joule law, whereby a current from an external power supply flows through a conductive material and is converted into thermal energy, according to the principle of conservation of energy. This thermal energy then raises the temperature of the conductive material. The temperature of the conductive material is directly proportional to its electrical conductivity. Therefore, high electrical conductivity is the key to combining EMI shielding and heating functions.

With the advantages of high applicability and facile fabrication methods, multifunctional EMI shielding with heating ability based

on conductive fabric or e-textile was still one of the priority selections [142–144]. Jia et al. prepared MXene-decorated wood-pulp fabric as a multifunctional EMI shielding with a Joule heating function [142]. As shown in Fig. 8a, the exfoliated $Ti_3C_2T_x$ MXene sheets were formed by etching Ti_3AlC_2 in an HCl/LiF mixture solution, followed by ultrasonication. The $Ti_3C_2T_x$ MXene nanosheets were deposited onto a wood-pulp fabric grid (FG) by vacuum filtration followed by hydrophobic methyltrimethoxysilane (MTMS) coating. As a result, a rough surface due to the covering of MXene nanosheets and the MTMS coating layer was observed. The MTMS-M/FG fabric with a thickness of ~0.5 mm showed an improved EMI SE from ~16.9 to ~34.6 and ~38.8 dB when MXene content increased from ~5.0 to ~9.3 and ~11.3 mg/cm^2, respectively. EMI SE reached a maximum of ~57.8 dB with a MXene content of ~14.5 mg/cm^2, meaning nearly 99.9999 % of incident EM waves are blocked. To achieve the higher EMI shielding performance, the MTMS-M/FG fabric layers with MXene content of ~9.3 mg/cm^2 were stacked together, and the EMI SE of 2 layers and 3 layers achieved ~69.5 and ~90.2 dB, respectively. Furthermore, the multifunctionality of MTMS-M/FG was demonstrated when it worked as a heater with the function of deicing or snow melting under a relatively low applied voltage, owing to its Joule-heating performance.

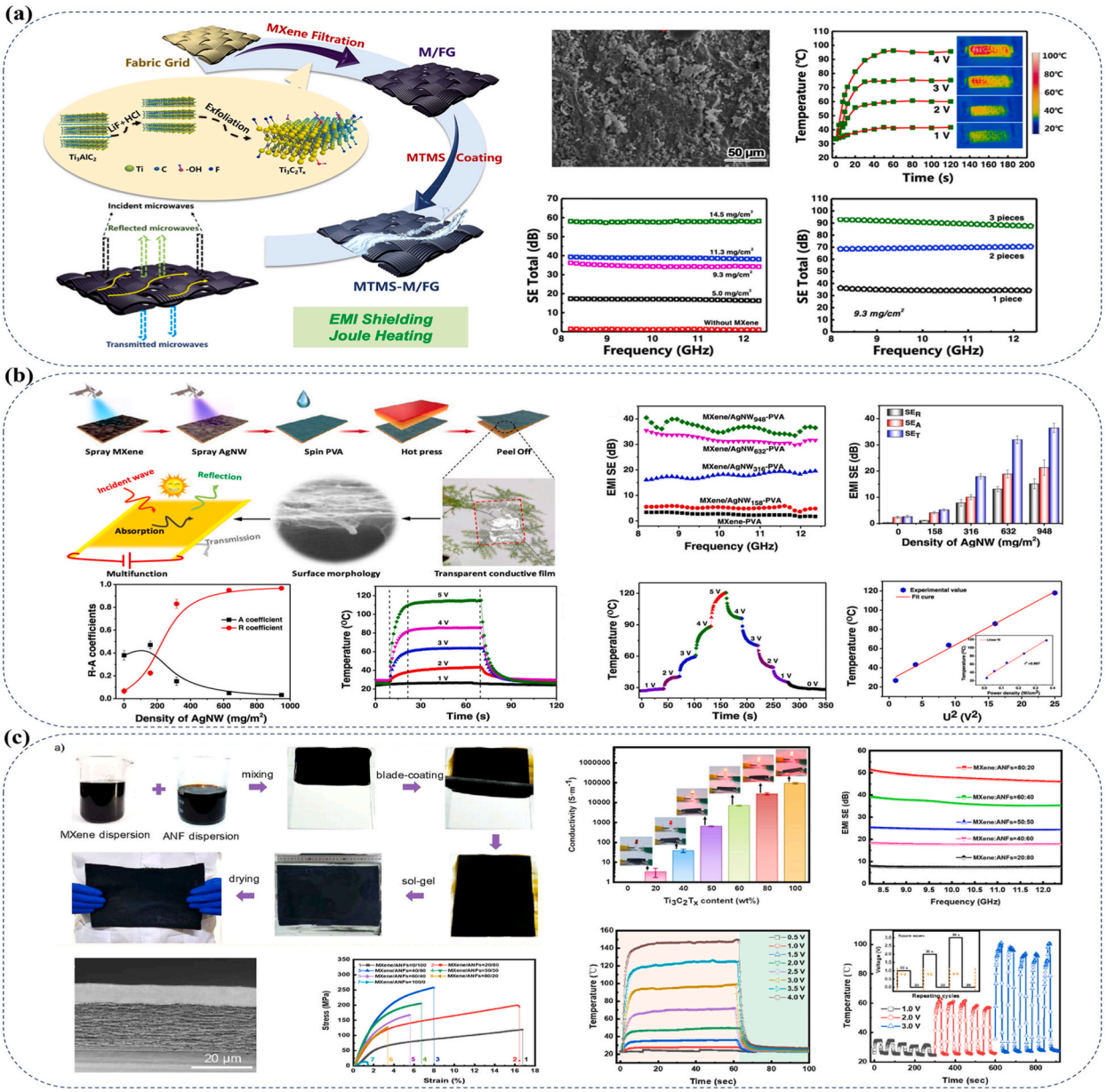

Fig. 8. Preparation procedures and characterization of EMI shielding materials with heating functions (a) A wood-pulp fabric grid/MXene/hydrophobic methyltrimethoxysilane fabric. Reproduced with permission from Ref. [142]. Copyright 2020 Elsevier Ltd. (b) MXene/silver nanowire/poly(vinyl alcohol) film composite. Reproduced with permission from Ref. [145]. Copyright 2020 American Chemical Society. (c) Large-scale, layered MXene/aramid nanofiber nanocomposite paper. Reproduced with permission from Ref. [146]. Copyright 2022 American Chemical Society.

The heater reached a saturated temperature of ~40–95 °C at an applied voltage of 1–4 V with thermal stability. This result was attributed to the outstanding electron-phonon interaction (EPI) of MXene nanosheets, allowing phonons to be dragged by electrons from low temperature to high temperature. Under the applied voltage, electrons actively move and excite phonons via scattering, resulting in a rapid increase in Joule heat.

Besides the strain sensing ability as discussed above, the multifunction EMI shielding textile based on $Ti_3C_2T_x$ MXene-coated cotton fabric in the research of Zhang et al. proved a good Joule heating performance with temperatures up to 150 °C at a supply voltage of only 6 V and good cyclic stability [9]. Zheng et al. also reported a Joule heating performance besides strain sensing ability of the multifunctional EMI shielding fabric based on RMCs with an increased temperature $\Delta T = 36.0$ °C and an applied voltage of 12 V [118]. Tian et al. reported another multifunctional textile, which was fabricated by alternatively depositing poly(sodium 4-styrene sulfonate) (PSS), and Chitosan adopted graphene on cotton fabric via layer-by-layer (LbL) electrostatic self-assembly [147]. The fabric possessed excellent EMI shielding performance, with a maximum EMI SE value of 30.04 dB in the frequency range of 30 MHz to 6 GHz. Its multifunctionality is demonstrated through its ability to work as a heater, where the temperature could increase by a ΔT_{max} of 134 °C within 8 min at a voltage of 7 V. In the report of Luo et al., a polypropylene (PP) fabric was decorated with Ag nanoparticles (NPs) by dipping in silver trifluoroacetate (STA) and treated with hydrazine, followed by spray-coating Fe_3O_4 NPs/polydimethylsiloxane (PDMS) [148]. Although the presence of Fe_3O_4/PDMS limited the electrical conductivity to 108.8 S/cm, the multifunctional fabric still achieved an EMI SE of ~56.1 dB with lower EM wave reflection in the X band and guaranteed excellent heating performance with a temperature of 79.3 °C under a voltage of 0.8 V and an area of 20 × 20 mm^2. Moreover, this fabric could absorb the light energy and transfer it into heat in the absence of electric power, owing to the photo-thermal effect. To fabricate a multifunctional EMI shielding fabric with heating ability, Bai et al. chose a facile and cost-effective method, which was coating a nickel–tungsten–phosphorus (Ni–W–P) ternary alloy on a polyamide (PA) textile by electroless plating technique [149]. The presence of W enhanced both thermal resistance and Joule heating properties; hence, the balance of the ratio between Ni (a magnetic metal) and W (a high impedance metal) resulted in excellent heating and EMI shielding performance. The fabric possessed an EMI SE of 43.6 dB in the frequency range 2–12.5 GHz with a thickness of ~117 μm and a heating temperature of up to 140 °C under 2 V within 60 s. Wang et al. reported a high EMI SE (~42 dB with a thickness of 0.43 mm) for silicone coated polypyrrole (PPy) modified MXene decorated polyethylene terephthalate (PET) textiles [150]. This exceptional EMI shielding performance of the textile is attributed to its excellent conductivity (~1000 S/m) due to the in situ polymerized PPy on MXene nanosheets. Furthermore, it led to a low voltage-driven Joule heating performance for multifunctional textiles (79 °C at 4 V, area of 4 × 1 cm^2).

Multifunctional EMI shielding materials with heating ability could also be fabricated as thin films for a variety of purposes [151, 152]. Zhou et al. reported a flexible MXene/AgNW-PVA film as a multifunctional EMI shielding with heating function [145]. As shown in Fig. 8b–a polycarbonate (PC) substrate was used as a template to orderly spray-coat $Ti_3C_2T_x$ MXene and AgNWs on top to construct sandwich-structure conductive networks. After that, the PVA layer was formed by a spin coating on the top of the hybrid conductive network. After hot-press treatment, the MXene/AgNW-PVA film could be peeled off from the PC substrate. The MXene/AgNW-PVA film could be loaded on the leaf of an asparagus fern, indicating that it was very light. The AgNW loading density (mg/m^2) determined the electrical conductivity and EMI shielding performance of the composite film. The EMI SE of the MXene/$AgNW_x$-PVA film (x is the loading density of AgNW) was enhanced with an increasing loading density of AgNW. The highest average EMI SE was 36.4 dB for the MXene/$AgNW_{948}$-PVA film, owing to its lowest sheet resistance of 4.4 Ω/sq, but with a relatively low transparency of 45 %. Obviously, SE_T, SE_A, and SE_R increased with the increasing AgNW content. The power impeded through reflection and absorption becomes apparent, with a rise in the silver nanowire (AgNW) content leading to an increased blockage of power through reflection, owing to enhanced conductivity. Initially, with a small amount of AgNW, the percolated conducting network could not be formed in MXene/AgNW-PVA, resulting in very small reflection. However, with the increase in AgNW loadings, the conductive network was more desired, and the reflection increased. The excellent Joule heating performance of MXene/$AgNW_{632}$-PVA film (20 × 20 mm^2) was observed. The heater increased the temperature rapidly under the applied voltages of 1–5 V and achieved a steady-state temperature (SST) of 27–114 °C within 10 s. The tailored temperature with applied DC voltage in real time indicated the excellent controllable Joule heating performance of the heater. Furthermore, the linear relationship between temperature and the square of the applied voltage demonstrated the controllability by varying the applied voltage of MXene/$AgNW_{632}$-PVA film. In addition, the heating efficiency of the MXene/$AgNW_{632}$-PVA film was found to be ~254 °C/(W.cm^2), which is comparable to or superior to that of other transparent films.

Similarly, by a combination of spray and spin coating, Zhou et al. fabricated multifunctional transparent EMI shielding films (TSFs) composed of MXene and Hf-SiO_2 on polycarbonate, which showed EMI SE of ~20 dB and Joule heating performance with a saturated temperature of ~100 °C at voltages of 13 V [153]. Various coating methods could be used to make multifunctional EMI shielding films. For example, Wu et al. coated silver nanoparticles (AgNPs)/(polystyrene-*block*-poly(ethylene-*co*-butylene)-*block*-polystyrene) (SEBS) on various substrates through the dripping method [121]. The 14.8 μm-thick coating layer provided multifunctionality with an EMI SE of 37.8 dB and a Joule heating-induced temperature of 80 °C in 60 s at a voltage of 1 V. UV-lithography and electroplating techniques were chosen by Han et al. to fabricate a multifunctional EMI shielding based on Cu/Cu_2O mesh-deposited glass [154]. It provided an EMI SE of ~24 dB in the Ku band and Joule heating up to 100 °C at a voltage of 3 V.

One of the most preferred methods to fabricate EMI-shielding thin films from colloidal nanomaterials is vacuum-assisted filtration. Zhan et al. used this method to deposit layer-by-layer (LBL) natural rubber/carbon nanotubes (NR/CNT) and natural rubber/hexagonal boron nitride (NR/*h*BN) to form a thin film [155]. The 1.4 mm thick (8 layers of NR/CNT-NR/*h*BN) film exhibited a specific EMI SE of 22.41 $dBmm^{-1}$ and a Joule heating-induced temperature of ~103 °C at a voltage of 2.5 V. The alternating multilayered structure was also used by Zhou et al. to concentrate MXene nanosheets together to form continuous conductive layers in a cellulose nanofiber/MXene (CNF@MXene) composite film by alternating vacuum filtration [7]. The 35 μm-thick CNF@MXene film exhibited EMI SE

of ~40 dB in the X-band and K-band while endowing Joule heating performance with saturated temperatures up to 100 °C at a voltage of 6 V within 10 s. Meanwhile, Li et al. mixed MXene nanosheets with montmorillonite (MMT) to form a uniform colloidal solution before filtrating by vacuum-assisted filtration [156]. The obtained MXene/MMT composite film containing 90 wt% MXene showed an EMI SE of 69 dB in the X-band with a thickness of only 25 μm. Furthermore, this film enables excellent Joule heating performance with a temperature up to 141 °C at an applied potential of 5 V and fast response (<10 s) due to the high electrical conductivity of 4420 S m^{-1}. Another structure, mimicking nacre, was developed by Sun et al. using suction filtration techniques to form a MXene/xanthan composite film [157]. In the microstructure of this composite film, MXene nanosheets played a role as bricks, and xanthan molecules served as mortar to mount MXene nanosheets in high order. This brick-and-mortar structure enhanced the electrical conductivity of the film up to 11,530 ± 176 S m^{-1} with 67 wt% of MXene, leading to an ultrahigh absolute shielding effectiveness (SSE/t = 14490.1 dB cm^2 g^{-1}) and excellent Joule heating performance (equilibrium temperatures of 105.1 °C at an applied voltage of 4 V). To form a dense film for enhancing mechanical properties with rigid structure, Liang et al. processed hot-pressing after vacuum-assisted filtration to make silver nanowires (AgNWs)/cellulose film [158]. Moreover, the in-plane alignment of AgNWs resulted in ultrahigh electrical conductivity (σ = 5571 S/cm), leading to an impressive EMI SE of 101 dB with a thickness of 44.5 μm, AgNWs of 50 wt%, and outstanding Joule heating performances (heating temperature of 99.5 °C, voltage of 2 V, area of 10 × 20 mm).

To make multifunctional EMI shielding films in production, some methods could be applied on a large scale. Ha et al. reported that a uniform graphene-PDMS composite film with a thickness of 500 μm and a graphene content of 8 wt% was fabricated using hot-pressing [159]. The film showed EMI SE of 25 dB and Joule heating performance with rapid heating from room temperature to 200 °C in 50 s that demonstrated fast de-icing ability. Li et al. mixed polyoxymethylene (POM) with multi-walled carbon nanotubes (MWCNT) and graphene nanoplates (GNP), then fabricated PMCNT and PMGNP composites, respectively, through a compression-molding process [160]. With the same thickness of 0.15 mm, the PMCNT (with 40 wt% MWCNT) and PMGNP (with 48 wt % GNP) films achieved EMI SE of 45.7 and 44.7 dB, respectively. In addition, these films demonstrated Joule heating performance by rapidly increasing the temperature up to 101.4 °C at a voltage of 3 V (in the case of PMCNT) and 107.6 °C at a voltage of 6 V (in the case of PMGNP). An aerogel film composed of aramid nanofibers (ANFs), carbon nanotubes (CNTs), and fluorocarbon (FC) resin, which is not only porous but also inherits the structure of a thin film, was developed via blade coating by Hu et al. [161]. The film exhibited an EMI SE of 54.4 dB in the X-band with a thickness of 568 μm. Besides, its good electrical conductivity (230 S m^{-1}) resulted in a Joule heating property with a temperature of 113.5 °C at 10 V. In a report about multifunctional EMI shielding based on metal nanowire networks (MNWs), Yang et al. used an electrodeposition technique to wrap nanowires of the silver nanowire (AgNW) network with reduced graphene oxide (rGO) to improve the conductivity of the network [162]. Owing to the enhancement of electrical conductivity (sheet resistance of 3.3 Ω/□), AgNW@rGO networks displayed an EMI SE up to 35.5 dB in the 8.2–12.4 GHz range, a high Joule heating temperature of 366 °C within 50 s at a voltage of 7 V, and good thermal stability. Wang et al. fabricated layered MXene/aramid nanofiber (ANF) nanocomposite papers using blade-coating and sol–gel conversion processes of dispersion solutions of the MXene and ANF mixture, as shown in Fig. 8c [146]. The strong connection between MXene and ANF led to a high tensile strength of 198.80 ± 5.35 MPa, a large strain of 15.30 ± 1.01 %, good flexibility, and continuous conductive paths inside the resultant composite with a maximum conductivity of 93063 ± 7914 S/m at a MXene content of 80 wt%. This composite paper showed an excellent EMI SE of 48 dB in the X-band and a specific shielding effectiveness of about 13188.2 dB $cm^2.g^{-1}$. In terms of Joule heating performance, the paper exhibited a fast thermal response of less than 10 s and a low driving voltage of less than 4 V, stability, and long-term working conditions.

3.5. Other functions

One of the important functions that can be easily integrated into multifunctional EMI materials is thermal management. Nanomaterials that act as active materials to block EM waves often have very good thermal conductivity [163,164]. Therefore, EMI materials can take advantage of this property to act as heat dissipation materials. Rajavel et al. reported a MXene-polyvinylidene fluoride (PVDF) nanocomposite film fabricated by the hot pressing method, which exhibited a remarkable EMI SE of 48.47 dB with 22.55 vol% MXene contents and a thickness of 2 mm [165]. The addition of MXene nanosheets enhanced the thermal conductivity of MXene/PVDF to 0.767 $Wm^{-1}K^{-1}$, significantly higher than that of pristine PVDF (0.18 $Wm^{-1}K^{-1}$). As a result, MXene/PVDF showed a quick temperature reduction in a cooling test due to the faster heat dissipation. MXene was also chosen by Jin et al. to be the filler in poly (vinyl alcohol) (PVA)/MXene film [3]. The film was fabricated by alternate drop casting PVA and MXene colloidal solution to form a layer-by-layer structure. The PVA/MXene film, composed of 19.5 wt% MXene content, showed excellent thermal and electrical conductivity, resulting in a maximum EMI SE of 44.4 dB with a thickness of 27 μm and an in-plane thermal conductivity coefficient of 4.57 W/mK. More than that, the film also exhibited flame retardancy and anti-dripping performance. The multifunctional EMI shielding MXene/MMT composite film, along with the heating function explained above, exhibited fire-resistant ability and anisotropic heat conduction with in-plane heat dissipation (a high in-plane thermal conductivity of 28.8 W $m^{-1}K^{-1}$) and cross-plane heat insulation (a low cross-plane thermal conductivity of 0.27 W/mK) [156]. Similarly, besides heating features, the multifunctional EMI shielding composites based on PMCNT and PMGNP in the report of Li et al. showed more functions, such as good thermal conductivities (1.95 $Wm^{-1}K^{-1}$ for PMCNT and 4.24 W $m^{-1}K^{-1}$ for PMGNP), solvent resistance, and anti-dripping. Jia et al. prepared a graphene/CNTs film in three steps: (i) vacuum filtration, (ii) hot-pressing carbonization, and (iii) graphitization at 2800 °C [2]. The film achieved an excellent EMI SE of 75 dB in the Ku-band with a thickness of 106 μm. Furthermore, the introduction of CNTs improved cross-plane thermal conductivity (6.27 W/m·K), while the graphitization process enhanced in-plane thermal conductivity (933.37 W/m·K), resulting in bidirectional thermal dissipation of the film. The multifunctional EMI shielding film based on AgNWs/cellulose developed by Liang et al., besides Joule heating properties, displayed an excellent in-plane thermal conductivity coefficient ($\lambda_{\parallel}$ =

10.55 W/mK) to dissipate heat accumulation [158]. Taking advantage of copper's good thermal and electrical conductivity through the hot-press molding method, Lee et al. fabricated a copper coated expanded polymer bead (EBCu)/poly(ε-caprolactone) (PCL) composite with dual functions, EMI shielding, and heat dissipation [166]. The composite composed of Cu content of ~9.8 vol% exhibited excellent EMI shielding (EMI SE of 110.7 dB at 7 GHz with a thickness of 1 mm) and thermal conductivity (7.0 $Wm^{-1}K^{-1}$). Fan et al. designed and fabricated a flexible multilayered composite film based on microfibrillated cellulose (MFC) and carbon nanotubes (CNT) (Fig. 9a) [167]. The dispersion solutions of MFC and CNT are alternatively vacuum-filtrated, followed by drying to form a multilayered composite film. The large-scale composite film showed excellent flexibility and was lightweight, even when folded into many types of shapes. When the CNT content was increased to 80 wt%, the EMI SE reached 28.87 dB. The EMI SE of M4C3 increased from 26.67 to 37.20 dB as the thickness increased from 36 to 110 μm. The thermal conductivity of M4C3 film showed high anisotropy, with cross-plane and in-plane TC of MC as high as 0.24 and 8.5 $Wm^{-1}K^{-1}$, respectively.

To protect EMI materials from external agents, such as weather, moisture, chemicals, dust, etc., these materials are often integrated with hydrophobic features. Along with EMI shielding, strain sensing, and Joule heating performance, in addition to providing EMI shielding, strain sensing, and Joule heating capabilities, a superhydrophobic element has been incorporated into the AgNP/SEBS-based coating [121]. This addition enhances the coating's effectiveness in preventing corrosion and ensuring durability, attributes attributed to the presence of SEBS. The self-powered strain sensing multifunctional EMI shielding based on PVDF-Ag-CNT/NWF fabric also exhibited good hydrophobicity (CÃ110.0°) and self-cleaning ability, protecting from rain and water [116]. Besides the electro-photo-thermal effect, Lou et al. demonstrated that their multifunctional EMI shielding fabric displayed super hydrophobicity

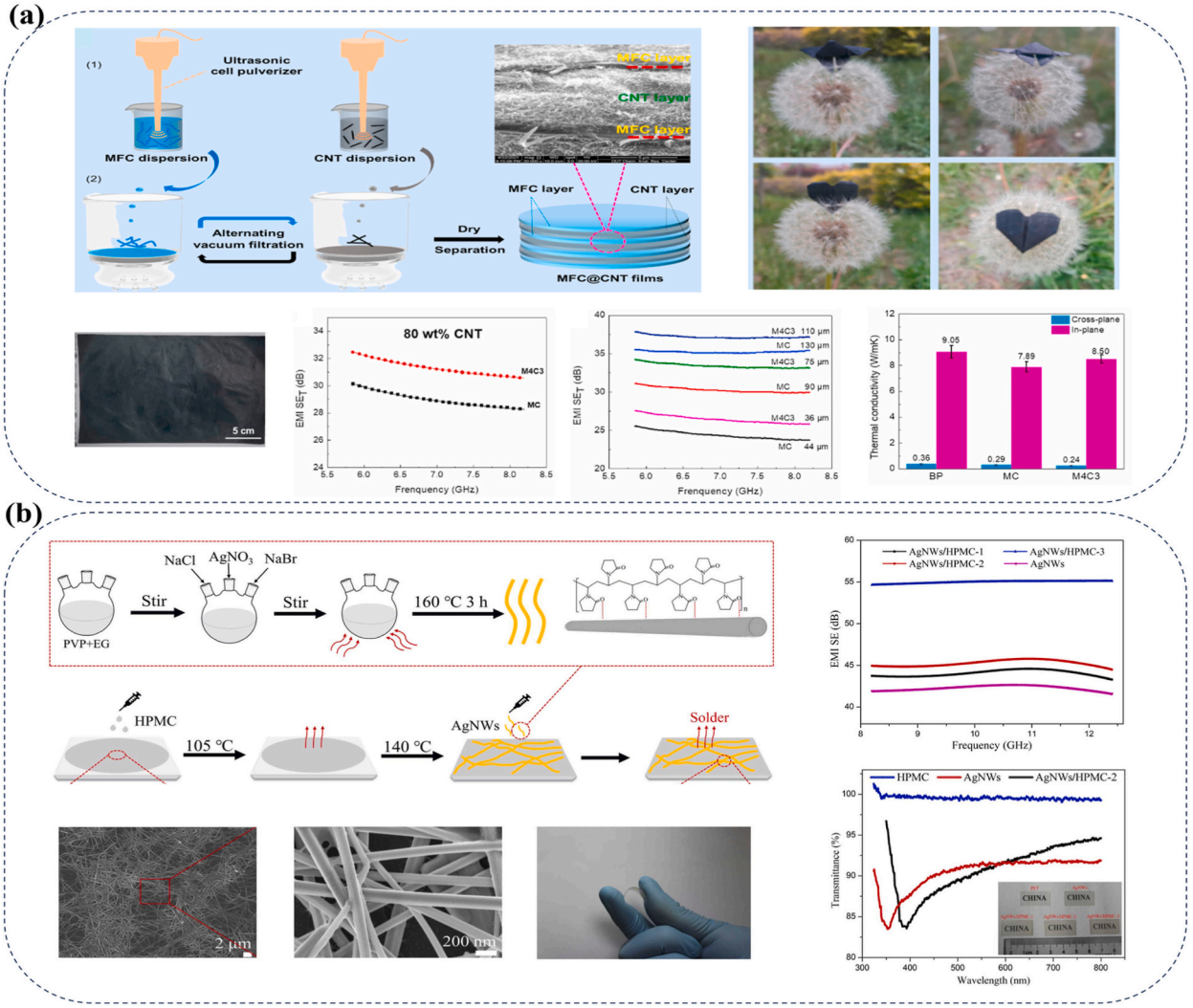

Fig. 9. Preparation procedures and characterization of EMI shielding materials with other functions (a) EMI shielding material with high EMI SE and thermal conductivity of multilayered microfibrillated cellulose/carbon nanotube composite film. Reproduced with permission from Ref. [167]. Copyright 2022 Elsevier Ltd. (b) Cellulose-wrapped silver nanowire-based transparent/EMI shielding film. Reproduced with permission from Ref. [168]. Copyright 2022 Elsevier B.V.

(CA = 151.1°) owing to the presence of PDMS, leading to excellent self-cleaning performance [148]. To enhance the hydrophobic properties of multifunctional EMI shielding materials, hydrophobic agents are often used. Wang et al. coated silicone oligomers on EMI shielding-heater textiles to provide a water-resistant function for wearable intelligent garments [150]. Hu et al. used a hydrophobic fluorocarbon (FC) resin to change the hydrophilicity of the ANF/CNT aerogel film [161]. The multifunctional EMI shielding based on FC-ANF/CNT hybrid aerogel film exhibits a self-cleaning feature thanks to its excellent hydrophobic property (CA up to 137.0°). A superhydrophobic property was also observed on PC/MXene/Hf-SiO_2 film, which is a multifunctional EMI shielding with Joule heating ability, in the report of Zhou et al. [153]. The superhydrophobic Hf-SiO_2 layer provided the film with a contact angle CA greater than 150.7°, resulting in excellent self-cleaning ability and resistance to environmental factors such as oxidation, water, chemicals, and dust. Interestingly, without hydrophobic agents, the MXene/Silver nanowire silk EMI shielding textile still achieved superhydrophobic property with a contact angle of 141.9° after aging five months under ambient conditions, despite its initial hydrophilic nature [134]. Liu et al. clarified that the alterations in surface properties during aging are attributed to the release of F groups from fractured Ti–F bonds in MXene. This process results in the formation of hydrophobic C–F bonds, ultimately giving rise to self-derived hydrophobicity.

EMI shielding materials with high optical transparency are desirable for visual optical windows or displays [32,153,169]. The key to developing optically transparent EMI shielding materials is highly transparent conductive materials. However, with the rising demand for flexible electronics, the brittleness and rigidity of current popular transparent conductive materials, such as ITO and FTO, no longer meet the requirements, leading to the search for alternative solutions. MXene has emerged as a potential candidate for transparent EMI shielding due to its metallic electrical conductivity and small light absorption. However, electromagnetic shielding efficiency and transparency are still on opposite sides. In the report of Zhou et al., the multifunctional EMI shielding film based on PC/MXene/Hf-SiO_2 film had to sacrifice its optical transparency (transmittance of only 33.4 % at a wavelength of 550 nm) to achieve EMI SE > 20 dB [152]. In their next research, they continued developing a multifunctional EMI shielding film based on MXene [145]. The supplementation of AgNW bridge-linked MXene nanosheets to form heterogeneous 1D/2D hybrid conductive networks in MXene/AgNW-PVA film led to an enhancement of both EMI shielding performance (EMI SE of 32 dB in the X-band) and transparency (transmittance of 52.3 % at a wavelength of 550 nm). In addition, the film worked as an electrical heater (described above) and can even warm itself without an electrical power supply due to a good photothermal response under light irradiation. Metallic mesh is also a significant candidate for transparent EMI shields because of its cost-saving, high transparency, and excellent conductivity. Han et al. reported an EMI SE of 24 dB when depositing Cu/Cu_2O mesh on a glass substrate to form a transparent EMI shielding-heater with a transmittance of ~82 % and reflectance of 8.7 % at a wavelength of 633 nm [154]. A flexible EMI shielding-heater film based on AgNW@rGO networks was developed by Yang et al., showing an average transmittance of 91.1 % [162]. Wang et al. found that an EMI shielding film made of Ag nanowires, ionic liquids, and thermoplastic polyurethane had an EMI SE of ~26.8 dB at 10 GHz and a transmittance of 67 % [170]. Zou et al. constructed a double-layered structure composed of cellulose-wrapped silver nanowire as a film, as shown in Fig. 9b [168]. The synthesized AgNWs were droplet-coated on a hydroxy propyl methyl cellulose (HPMC)/PET structure and then dried at 140 °C to form AgNWs/HPMC film. The strong hydrogen bond and adhesion force between AgNWs and HPMC resulted in improvements in the continuous conductive network of composites, high flexibility, and oxidation resistance. They observed that a high transmittance of 90.55 % at 550 nm and an EMI SE of 45.79 dB in the X band were attained.

In addition, numerous other studies have endowed multifunctional EMI shielding materials with diverse functions and broadened their field of application. Zhang et al. coated polyaniline (PANI) on cotton fibers through an in situ polymerization process to form a flexible EMI shielding cloth with additional features such as improved UV-VIS absorption, high tensile strength, and particularly gas sensing [171]. The gas sensing properties of these materials showed high selectivity for NH_3, fast response, short recovery time (20.1s), repeatability, and stability even under bending conditions. The multifunctional EMI shielding fabric based on RMC developed by Zheng et al., besides strain sensing and Joule heating functions as discussed above, could also play a role as a flexible all-solid-state supercapacitor electrode with a high specific capacitance of 383.3 F g^{-1} (or 258 mF cm^{-2}) [118]. Interestingly, Zhang et al. integrated energy-havesting capability into a stretchable EMI shielding material called the EMI shielding hybrid nanogenerator (ES-HNG) [117]. This material would scavenge thermal and mechanical energy based on triboelectric, piezoelectric, and pyroelectric effects. Another function of this ES-HNG is a self-powered strain sensor, as mentioned in the previous part. Especially, the strain sensor-EMI shielding based on Ni@PET-g-PAO/Fe_3O_4 fabric exhibited a magnetic response characteristic owing to the introduction of Fe_3O_4 NPs [113]. The fabric could be used as a non-contact magnetoelectric switch. Enhancing mechanical properties and environmental resistance were also noticed for the EMI shielding material in the report of Jia et al. [123]. The combination of GO with AgNW protected the material from corrosive agents and improved its bending endurance. Obviously, there is a trade-off between EMI shielding performance and added features in multifunctional EMI shielding materials.

4. Conclusions and perspectives

The proliferation of electromagnetic waves is probably inevitable at this moment and in the future. Therefore, studies on the EMI shielding properties of materials need to be extensively explored. Research aimed at increasing EM wave absorption and reducing EM wave reflection at the surface of EMI shielding materials is an urgent trend. In addition, the general properties required for EMI shielding materials, such as high shielding effectiveness, lightweight, flexibility, high mechanical properties, low cost, facile process, etc., also need to be further developed.

The multifunctional EMI shielding materials with additional functions beyond EMI shielding are still in their infancy but have initially shown promising signals and great potential. As a result, there are still many opportunities and fundamental questions to be explored. Depending on the intended application, multifunctional electromagnetic wave shields need to be equipped with specific properties. This report summarized and categorized the most recent advances in EMI shielding with additional functions including

strain sensing, humidity sensing, temperature sensing, heating, thermal conductivity, heat dissipation, hydrophobicity (self-cleaning, environment resistance, such as oxidation, water, chemicals, and dust), transparence, gas sensing (NH_3), flame retardancy and anti-dripping, photothermal (self-warm), supercapacitor electrodes, and nanogenerator.

From the point of view of material science and applications, we would like to propose the following potential research directions for multifunctional EMI shielding materials in the future:

Composite materials may be the key to unlocking the features of multifunctional EMI shielding materials by combining different relevant and desirable features of nanomaterials to form a new material with broad properties. Especially for the nanocomposites based on MXene, as MXene itself is already a super material with many properties and applications that have been announced. Moreover, the EMI shielding property of MXene is at the forefront of all materials. Hence, effectively using the properties of the MXene in combination with other nanomaterials, such as graphene, CNTs, etc., to form nanocomposite can open new functions for materials while maintaining a high EMI shielding performance. We strongly suggest that the development of multifunctional EMI shielding based on MXene nanocomposites will continue to thrive for many more years, especially if the oxidation stability of MXene is enhanced. Besides, the composite based on cellulose nanofibers also attracts more attention due to its natural resources, high elastic modulus, high strength, low density, and low thermal expansion for diverse applications.

The multifunctional EMI shielding textile is an attractive alternative to currently used conductive wires and dyes for smart garments, sensors, actuators, energy generators, and EMI shielding applications. Enabling a widespread implementation of seamlessly integrated textile-based multifunctional EMI shielding can greatly improve noninvasive healthcare by monitoring the physiological states of sweat (humidity sensing), human motion (strain sensing), keeping the body warm (heating), and providing maximum EMI shielding performance in military personnel, industrial workers, pregnant women, hospital workers, etc. Furthermore, multifunctional EMI shielding textiles with nanogenerator functionality that can utilize human body heat, humidity, movement, and solar power for energy harvesting are another promising sector for efficient and alternative sources of energy at inaccessible locations, low Earth orbit, space, robotics, etc.

In addition, we propose some features for multifunctional EMI shielding materials when considering the demand for practical applications. A transparent multifunctional EMI shield with a touch-screen feature that can be used in display applications. In electronic devices equipped with a touch screen, EM waves generated during operation of the devices can transmit through the touch screen, causing malfunction of other devices and a detrimental effect on human health simultaneously, or penetrating through the touch screen to damage the device by external EM waves. Therefore, the touch screen should be equipped with EMI shielding features. Similarly, the combination of the EMI shielding feature with the electrochromic property on smart windows endows a protection solution from both UV radiation, heat from IR radiation, and harmful EM waves. Remarkably, EMI shielding materials with healing properties (shape memory effect) have been studied for their useful applications in biomedical fields such as tissue engineering, neurosurgical stents, implanted cardioverter defibrillators, etc. For example, the shape-memory integrated EMI shielding composite material could be used for precise devices like pacemakers. This application is crucial to avoid damage to other organs by controlling their size during surgical procedures. Simultaneously, it prevents EM radiation from damaging the working status through interruptions or malfunctions of implanted equipment in human emergency cases. Several works showed the promise of these kinds of functional materials, but their EMI performance is still low (~30 dB) or the thickness is large (500 μm, ~50 dB) [172–175]. We expect researchers to focus on the EMI shielding ability of devices while maintaining enough healing properties by improving the interfacial connection between fillers and shape-memory polymers of flexible-compatible composite films, or high-power density for triboelectric nanogenerators [176].

Ethics statement

Informed consent was not required for this study because this study is based exclusively on published literature.

Notes

The authors declare no competing financial interest.

Data availability statement

No. Data included in article/supp. material/referenced in article.

CRediT authorship contribution statement

Quy-Dat Nguyen: Writing – review & editing, Writing – original draft, Resources, Investigation, Formal analysis, Data curation. **Choon-Gi Choi:** Writing – review & editing, Writing – original draft, Resources, Project administration, Funding acquisition, Conceptualization.

Declaration of competing interest

The authors declare that they have no known competing financial interests or personal relationships that could have appeared to influence the work reported in this paper.

Acknowledgment

This work was supported by the Korea Evaluation Institute of Industrial Technology (KEIT) grant funded by the Korea government (MOTIE) (20013138).

References

[1] M.H. Alsharif, A. Hilary Kelechi, M.A. Albreem, S. Ashraf Chaudhry, M. Sultan Zia, S. Kim, S S Review Sixth Generation (6G) Wireless Networks: Vision, Research Activities, Challenges and Potential Solutions, (n.d.). https://doi.org/10.3390/sym12040676..
[2] H. Jia, Q.Q. Kong, X. Yang, L.J. Xie, G.H. Sun, L.L. Liang, J.P. Chen, D. Liu, Q.G. Guo, C.M. Chen, Dual-functional graphene/carbon nanotubes thick film: bidirectional thermal dissipation and electromagnetic shielding, Carbon N Y 171 (2021) 329–340, https://doi.org/10.1016/J.CARBON.2020.09.017.
[3] X. Jin, J. Wang, L. Dai, X. Liu, L. Li, Y. Yang, Y. Cao, W. Wang, H. Wu, S. Guo, Flame-retardant poly(vinyl alcohol)/MXene multilayered films with outstanding electromagnetic interference shielding and thermal conductive performances, Chem. Eng. J. 380 (2020) 122475, https://doi.org/10.1016/J.CEJ.2019.122475.
[4] F. Shahzad, M. Alhabeb, C.B. Hatter, B. Anasori, S.M. Hong, C.M. Koo, Y. Gogotsi, Electromagnetic interference shielding with 2D transition metal carbides (MXenes), Science 353 (2016) (1979) 1137–1140, https://doi.org/10.1126/SCIENCE.AAG2421/SUPPL_FILE/SHAHZAD.SM.PDF.
[5] R. Yang, X. Gui, L. Yao, Q. Hu, L. Yang, H. Zhang, Y. Yao, H. Mei, Z. Tang, Ultrathin, lightweight, and flexible CNT buckypaper enhanced using MXenes for electromagnetic interference shielding, Nano-Micro Lett. 13 (2021), https://doi.org/10.1007/S40820-021-00597-4.
[6] F. Xie, F. Jia, L. Zhuo, Z. Lu, L. Si, J. Huang, M. Zhang, Q. Ma, Ultrathin MXene/aramid nanofiber composite paper with excellent mechanical properties for efficient electromagnetic interference shielding, Nanoscale 11 (2019) 23382–23391, https://doi.org/10.1039/C9NR07331K.
[7] B. Zhou, Z. Zhang, Y. Li, G. Han, Y. Feng, B. Wang, D. Zhang, J. Ma, C. Liu, Flexible, robust, and multifunctional electromagnetic interference shielding film with alternating cellulose nanofiber and MXene layers, ACS Appl. Mater. Interfaces 12 (2020) 4895–4905, https://doi.org/10.1021/ACSAMI.9B19768/ASSET/IMAGES/LARGE/AM9B19768_0002.JPEG.
[8] J. Liu, S. Lin, K. Huang, C. Jia, Q. Wang, Z. Li, J. Song, Z. Liu, H. Wang, M. Lei, H. Wu, A large-area AgNW-modified textile with high-performance electromagnetic interference shielding, (n.d.). https://doi.org/10.1038/s41528-020-0074-0..
[9] X. Zhang, X. Wang, Z. Lei, L. Wang, M. Tian, S. Zhu, H. Xiao, X. Tang, L. Qu, Flexible MXene-decorated fabric with interwoven conductive networks for integrated joule heating, electromagnetic interference shielding, and strain sensing performances, ACS Appl. Mater. Interfaces 12 (2020) 14459–14467, https://doi.org/10.1021/ACSAMI.0C01182/ASSET/IMAGES/LARGE/AM0C01182_0005.JPEG.
[10] B. Anasori, Y. Gogotsi, 2D Metal Carbides and Nitrides (MXenes): Structure, Properties and Applications, 2D Metal Carbides and Nitrides (MXenes): Structure, Properties and Applications, 2019, pp. 1–534, https://doi.org/10.1007/978-3-030-19026-2.
[11] A. Iqbal, J. Kwon, M.K. Kim, C.M. Koo, MXenes for electromagnetic interference shielding: experimental and theoretical perspectives, Mater Today Adv 9 (2021) 100124, https://doi.org/10.1016/J.MTADV.2020.100124.
[12] T. Yun, H. Kim, A. Iqbal, Y. Soo Cho, G. San Lee, M.-K. Kim, S. Joon Kim, D. Kim, Y. Gogotsi, S. Ouk Kim, C. Min Koo, T. Yun, G.S. Lee, S.O. Kim, H. Kim, A. Iqbal, Y.S. Cho, S.J. Kim, D. Kim, C.M. Koo, M. Kim, Y. Gogotsi, Electromagnetic shielding of monolayer MXene assemblies, Adv. Mater. 32 (2020) 1906769, https://doi.org/10.1002/ADMA.201906769.
[13] S. Geetha, K.K.S. Kumar, C.R.K. Rao, M. Vijayan, D.C. Trivedi, EMI shielding: methods and materials—a review, J. Appl. Polym. Sci. 112 (2009) 2073–2086, https://doi.org/10.1002/APP.29812.
[14] K. Song, F.S. Pan, X.H. Chen, Z.H. Zhang, A.T. Tang, J. She, Z.W. Yu, H.C. Pan, X.Y. Xu, Effect of texture on the electromagnetic shielding property of magnesium alloy, Mater. Lett. 157 (2015) 73–76, https://doi.org/10.1016/J.MATLET.2015.05.017.
[15] L. Liu, X. Chen, F. Pan, A. Tang, X. Wang, J. Liu, S. Gao, Microstructure, texture, mechanical properties and electromagnetic shielding effectiveness of Mg–Zn–Zr–Ce alloys, Mater. Sci. Eng., A 669 (2016) 259–268, https://doi.org/10.1016/J.MSEA.2016.05.098.
[16] L. Liu, X. Chen, J. Wang, L. Qiao, S. Gao, K. Song, C. Zhao, X. Liu, D. Zhao, F. Pan, Effects of Y and Zn additions on electrical conductivity and electromagnetic shielding effectiveness of Mg-Y-Zn alloys, J. Mater. Sci. Technol. 35 (2019) 1074–1080, https://doi.org/10.1016/J.JMST.2018.12.010.
[17] R. Pandey, S. Tekumalla, M. Gupta, Magnesium-iron micro-composite for enhanced shielding of electromagnetic pollution, Compos. B Eng. 163 (2019) 150–157, https://doi.org/10.1016/J.COMPOSITESB.2018.11.038.
[18] J.H. Park, J.W. Lee, H.J. Choi, W.G. Jang, T.S. Kim, D.S. Suh, H.Y. Jeong, S.Y. Chang, J.C. Roh, C.S. Yoo, K.H. Kim, C. Park, S.J. Suh, Electromagnetic interference shielding effectiveness of sputtered NiFe/Cu multi-layer thin film at high frequencies, Thin Solid Films 677 (2019) 130–136, https://doi.org/10.1016/J.TSF.2019.03.015.
[19] Z. Xu, H. Hao, Electromagnetic interference shielding effectiveness of aluminum foams with different porosity, J. Alloys Compd. 617 (2014) 207–213, https://doi.org/10.1016/J.JALLCOM.2014.07.188.
[20] R. Kumar, H. Jain, S. Sriram, A. Chaudhary, A. Khare, V.A.N. Ch, D.P. Mondal, Lightweight open cell aluminum foam for superior mechanical and electromagnetic interference shielding properties, Mater. Chem. Phys. 240 (2020) 122274, https://doi.org/10.1016/J.MATCHEMPHYS.2019.122274.
[21] P.S. Liu, H.B. Qing, H.L. Hou, Y.Q. Wang, Y.L. Zhang, EMI shielding and thermal conductivity of a high porosity reticular titanium foam, Mater. Des. 92 (2016) 823–828, https://doi.org/10.1016/J.MATDES.2015.12.105.
[22] Y. Lu, Q. Liang, W. Li, Fabrication of copper/modal fabric composites through electroless plating process for electromagnetic interference shielding, Mater. Chem. Phys. 140 (2013) 553–558, https://doi.org/10.1016/J.MATCHEMPHYS.2013.03.068.
[23] H. Zhao, L. Hou, Y. Lu, Electromagnetic shielding effectiveness and serviceability of the multilayer structured cuprammonium fabric/polypyrrole/copper (CF/PPy/Cu) composite, Chem. Eng. J. 297 (2016) 170–179, https://doi.org/10.1016/J.CEJ.2016.04.004.
[24] Y. Lu, L. Xue, Electromagnetic interference shielding, mechanical properties and water absorption of copper/bamboo fabric (Cu/BF) composites, Compos. Sci. Technol. 72 (2012) 828–834, https://doi.org/10.1016/J.COMPSCITECH.2012.02.012.
[25] T.B. Yang, J.Y. Zong, H. Lin, D.X. Yan, J. Lei, Z.M. Li, Stretchable textile with ultra-high electromagnetic interference shielding performance based on porous wrinkled conductive network, Chem. Eng. J. 476 (2023) 146570, https://doi.org/10.1016/J.CEJ.2023.146570.
[26] T.W. Shyr, J.W. Shie, Electromagnetic shielding mechanisms using soft magnetic stainless steel fiber enabled polyester textiles, J. Magn. Magn Mater. 324 (2012) 4127–4132, https://doi.org/10.1016/J.JMMM.2012.07.037.
[27] S.S. Tzeng, F.Y. Chang, EMI shielding effectiveness of metal-coated carbon fiber-reinforced ABS composites, Mater. Sci. Eng., A 302 (2001) 258–267, https://doi.org/10.1016/S0921-5093(00)01824-4.
[28] C. Xia, J. Yu, S.Q. Shi, Y. Qiu, L. Cai, H.F. Wu, H. Ren, X. Nie, H. Zhang, Natural fiber and aluminum sheet hybrid composites for high electromagnetic interference shielding performance, Compos. B Eng. 114 (2017) 121–127, https://doi.org/10.1016/J.COMPOSITESB.2017.01.044.
[29] N. Zhang, R. Zhao, D. He, Y. Ma, J. Qiu, C. Jin, C. Wang, Lightweight and flexible Ni-Co alloy nanoparticle-coated electrospun polymer nanofiber hybrid membranes for high-performance electromagnetic interference shielding, J. Alloys Compd. 784 (2019) 244–255, https://doi.org/10.1016/J.JALLCOM.2018.12.341.
[30] G.A. Gelves, M.H. Al-Saleh, U. Sundararaj, Highly electrically conductive and high performance EMI shielding nanowire/polymer nanocomposites by miscible mixing and precipitation, J. Mater. Chem. 21 (2010) 829–836, https://doi.org/10.1039/C0JM02546A.
[31] T.W. Lee, S.E. Lee, Y.G. Jeong, Highly effective electromagnetic interference shielding materials based on silver nanowire/cellulose papers, ACS Appl. Mater. Interfaces 8 (2016) 13123–13132, https://doi.org/10.1021/ACSAMI.6B02218/ASSET/IMAGES/AM-2016-02218T_M012.GIF.
[32] L.C. Jia, D.X. Yan, X. Liu, R. Ma, H.Y. Wu, Z.M. Li, Highly efficient and reliable transparent electromagnetic interference shielding film, ACS Appl. Mater. Interfaces 10 (2018) 11941–11949, https://doi.org/10.1021/ACSAMI.8B00492/ASSET/IMAGES/LARGE/AM-2018-004926_0005. JPEG.

[33] M. Hu, J. Gao, Y. Dong, K. Li, G. Shan, S. Yang, R.K.Y. Li, Flexible transparent PES/silver nanowires/PET sandwich-structured film for high-efficiency electromagnetic interference shielding, Langmuir 28 (2012) 7101–7106, https://doi.org/10.1021/LA300720Y/SUPPL_FILE/LA300720Y_SI_001.PDF.
[34] J. Li, W.J. Peng, Z.J. Fu, X.H. Tang, H. Wu, S. Guo, M. Wang, Achieving high electrical conductivity and excellent electromagnetic interference shielding in poly(lactic acid)/silver nanocomposites by constructing large-area silver nanoplates in polymer matrix, Compos. B Eng. 171 (2019) 204–213, https://doi.org/10.1016/J.COMPOSITESB.2019.05.003.
[35] P. Sambyal, S.J. Noh, J.P. Hong, W.N. Kim, A. Iqbal, S.S. Hwang, S.M. Hong, C.M. Koo, FeSiAl/metal core shell hybrid composite with high-performance electromagnetic interference shielding, Compos. Sci. Technol. 172 (2019) 66–73, https://doi.org/10.1016/J.COMPSCITECH.2019.01.007.
[36] H. Wang, K. Zheng, X. Zhang, T. Du, C. Xiao, X. Ding, C. Bao, L. Chen, X. Tian, Segregated poly(vinylidene fluoride)/MWCNTs composites for high-performance electromagnetic interference shielding, Compos Part A Appl Sci Manuf 90 (2016) 606–613, https://doi.org/10.1016/J.COMPOSITESA.2016.08.030.
[37] H. Li, D. Yuan, P. Li, C. He, High conductive and mechanical robust carbon nanotubes/waterborne polyurethane composite films for efficient electromagnetic interference shielding, Compos Part A Appl Sci Manuf 121 (2019) 411–417, https://doi.org/10.1016/J.COMPOSITESA.2019.04.003.
[38] K. Zhang, G.H. Li, L.M. Feng, N. Wang, J. Guo, K. Sun, K.X. Yu, J.B. Zeng, T. Li, Z. Guo, M. Wang, Ultralow percolation threshold and enhanced electromagnetic interference shielding in poly(l -lactide)/multi-walled carbon nanotube nanocomposites with electrically conductive segregated networks, J Mater Chem C Mater 5 (2017) 9359–9369, https://doi.org/10.1039/C7TC02948A.
[39] L.C. Jia, M.Z. Li, D.X. Yan, C.H. Cui, H.Y. Wu, Z.M. Li, A strong and tough polymer–carbon nanotube film for flexible and efficient electromagnetic interference shielding, J Mater Chem C Mater 5 (2017) 8944–8951, https://doi.org/10.1039/C7TC02259J.
[40] M. Arjmand, M. Mahmoodi, G.A. Gelves, S. Park, U. Sundararaj, Electrical and electromagnetic interference shielding properties of flow-induced oriented carbon nanotubes in polycarbonate, Carbon N Y 49 (2011) 3430–3440, https://doi.org/10.1016/J.CARBON.2011.04.039.
[41] M. Mahmoodi, M. Arjmand, U. Sundararaj, S. Park, The electrical conductivity and electromagnetic interference shielding of injection molded multi-walled carbon nanotube/polystyrene composites, Carbon N Y 50 (2012) 1455–1464, https://doi.org/10.1016/J.CARBON.2011.11.004.
[42] J. Jyoti, S. Basu, B.P. Singh, S.R. Dhakate, Superior mechanical and electrical properties of multiwall carbon nanotube reinforced acrylonitrile butadiene styrene high performance composites, Compos. B Eng. 83 (2015) 58–65, https://doi.org/10.1016/J.COMPOSITESB.2015.08.055.
[43] P. Verma, P. Saini, R.S. Malik, V. Choudhary, Excellent electromagnetic interference shielding and mechanical properties of high loading carbon-nanotubes/polymer composites designed using melt recirculation equipped twin-screw extruder, Carbon N Y 89 (2015) 308–317, https://doi.org/10.1016/J.CARBON.2015.03.063.
[44] L.C. Jia, D.X. Yan, C.H. Cui, X. Jiang, X. Ji, Z.M. Li, Electrically conductive and electromagnetic interference shielding of polyethylene composites with devisable carbon nanotube networks, J Mater Chem C Mater 3 (2015) 9369–9378, https://doi.org/10.1039/C5TC01822F.
[45] G.P. Kar, S. Biswas, S. Bose, Simultaneous enhancement in mechanical strength, electrical conductivity, and electromagnetic shielding properties in PVDF–ABS blends containing PMMA wrapped multiwall carbon nanotubes, Phys. Chem. Chem. Phys. 17 (2015) 14856–14865, https://doi.org/10.1039/C5CP01452B.
[46] F. Ren, Z. Li, L. Xu, Z. Sun, P. Ren, D. Yan, Z. Li, Large-scale preparation of segregated PLA/carbon nanotube composite with high efficient electromagnetic interference shielding and favourable mechanical properties, Compos. B Eng. 155 (2018) 405–413, https://doi.org/10.1016/J.COMPOSITESB.2018.09.030.
[47] H.Y. Wu, L.C. Jia, D.X. Yan, J. feng Gao, X.P. Zhang, P.G. Ren, Z.M. Li, Simultaneously improved electromagnetic interference shielding and mechanical performance of segregated carbon nanotube/polypropylene composite via solid phase molding, Compos. Sci. Technol. 156 (2018) 87–94, https://doi.org/10.1016/J.COMPSCITECH.2017.12.027.
[48] W.C. Yu, J.Z. Xu, Z.G. Wang, Y.F. Huang, H.M. Yin, L. Xu, Y.W. Chen, D.X. Yan, Z.M. Li, Constructing highly oriented segregated structure towards high-strength carbon nanotube/ultrahigh-molecular-weight polyethylene composites for electromagnetic interference shielding, Compos Part A Appl Sci Manuf 110 (2018) 237–245, https://doi.org/10.1016/J.COMPOSITESA.2018.05.004.
[49] W.C. Yu, G.Q. Zhang, Y.H. Liu, L. Xu, D.X. Yan, H.D. Huang, J.H. Tang, J.Z. Xu, Z.M. Li, Selective electromagnetic interference shielding performance and superior mechanical strength of conductive polymer composites with oriented segregated conductive networks, Chem. Eng. J. 373 (2019) 556–564, https://doi.org/10.1016/J.CEJ.2019.05.074.
[50] Y.F. Liu, L.M. Feng, Y.F. Chen, Y.D. Shi, X.D. Chen, M. Wang, Segregated polypropylene/cross-linked poly(ethylene-co-1-octene)/multi-walled carbon nanotube nanocomposites with low percolation threshold and dominated negative temperature coefficient effect: towards electromagnetic interference shielding and thermistors, Compos. Sci. Technol. 159 (2018) 152–161, https://doi.org/10.1016/J.COMPSCITECH.2018.02.041.
[51] Y.J. Yim, K.Y. Rhee, S.J. Park, Electromagnetic interference shielding effectiveness of nickel-plated MWCNTs/high-density polyethylene composites, Compos. B Eng. 98 (2016) 120–125, https://doi.org/10.1016/J.COMPOSITESB.2016.04.061.
[52] B.J. Kim, K.M. Bae, Y.S. Lee, K.H. An, S.J. Park, EMI shielding behaviors of Ni-coated MWCNTs-filled epoxy matrix nanocomposites, Surf. Coat. Technol. 242 (2014) 125–131, https://doi.org/10.1016/J.SURFCOAT.2014.01.030.
[53] Y. Liu, D. Song, C. Wu, J. Leng, EMI shielding performance of nanocomposites with MWCNTs, nanosized Fe3O4 and Fe, Compos. B Eng. 63 (2014) 34–40, https://doi.org/10.1016/J.COMPOSITESB.2014.03.014.
[54] V. Bhingardive, S. Suwas, S. Bose, New physical insights into the electromagnetic shielding efficiency in PVDF nanocomposites containing multiwall carbon nanotubes and magnetic nanoparticles, RSC Adv. 5 (2015) 79463–79472, https://doi.org/10.1039/C5RA13901E.
[55] M.Y. Li, S. Gupta, C. Chang, N.H. Tai, Layered hybrid composites using multi-walled carbon nanotube film as reflection layer and multi-walled carbon nanotubes/neodymium magnet/epoxy as absorption layer perform selective electromagnetic interference shielding, Compos. B Eng. 161 (2019) 617–626, https://doi.org/10.1016/J.COMPOSITESB.2018.12.130.
[56] X. Lei, X. Zhang, A. Song, S. Gong, Y. Wang, L. Luo, T. Li, Z. Zhu, Z. Li, Investigation of electrical conductivity and electromagnetic interference shielding performance of Au@CNT/sodium alginate/polydimethylsiloxane flexible composite, Compos Part A Appl Sci Manuf 130 (2020) 105762, https://doi.org/10.1016/J.COMPOSITESA.2019.105762.
[57] F. Yang, S. Ma, C.M. Khor, Y. Su, Z. Barani, Z. Xu, A. Boyko, A. Iddya, N. Segev-Mark, X. Rayne Zheng, F. Kargar, A.A. Balandin, G. Ramon, I. De Rosa, E. Hoek, D. Jassby, One-step method for the fabrication of pure and metal-decorated densified CNT films for effective electromagnetic interference shielding, Carbon N Y 214 (2023) 118370, https://doi.org/10.1016/J.CARBON.2023.118370.
[58] Y. Wu, S. Tan, G. Fang, Y. Zhang, G. Ji, Manipulating CNT films with atomic precision for absorption effectiveness–enhanced electromagnetic interference shielding and adaptive infrared camouflage, Adv. Funct. Mater. (2024) 2402193, https://doi.org/10.1002/ADFM.202402193.
[59] P. Nimbalkar, A. Korde, R.K. Goyal, Electromagnetic interference shielding of polycarbonate/GNP nanocomposites in X-band, Mater. Chem. Phys. 206 (2018) 251–258, https://doi.org/10.1016/J.MATCHEMPHYS.2017.12.027.
[60] W. Zhang, L. Wei, J. Ma, S.L. Bai, Exfoliation and defect control of graphene oxide for waterborne electromagnetic interference shielding coatings, Compos Part A Appl Sci Manuf 132 (2020) 105838, https://doi.org/10.1016/J.COMPOSITESA.2020.105838.
[61] L. Wei, W. Zhang, J. Ma, S.L. Bai, Y. Ren, C. Liu, D. Simion, J. Qin, π-π stacking interface design for improving the strength and electromagnetic interference shielding of ultrathin and flexible water-borne polymer/sulfonated graphene composites, Carbon N Y 149 (2019) 679–692, https://doi.org/10.1016/J.CARBON.2019.04.058.
[62] S.T. Hsiao, C.C.M. Ma, H.W. Tien, W.H. Liao, Y.S. Wang, S.M. Li, C.Y. Yang, S.C. Lin, R. Bin Yang, Effect of covalent modification of graphene nanosheets on the electrical property and electromagnetic interference shielding performance of a water-borne polyurethane composite, ACS Appl. Mater. Interfaces 7 (2015) 2817–2826, https://doi.org/10.1021/AM508069V/SUPPL_FILE/AM508069V_SI_001.PDF.
[63] S.T. Hsiao, C.C.M. Ma, W.H. Liao, Y.S. Wang, S.M. Li, Y.C. Huang, R. Bin Yang, W.F. Liang, Lightweight and flexible reduced graphene oxide/water-borne polyurethane composites with high electrical conductivity and excellent electromagnetic interference shielding performance, ACS Appl. Mater. Interfaces 6 (2014) 10667–10678, https://doi.org/10.1021/AM502412Q/SUPPL_FILE/AM502412Q_SI_001.PDF.
[64] G. George, S.M. Simon, V. Prakashan, M. Sajna, M. Faisal, R. Wilson, A. Chandran, P.R. Biju, C. Joseph, N.V. Unnikrishnan, Green and facile approach to prepare polypropylene/in situ reduced graphene oxide nanocomposites with excellent electromagnetic interference shielding properties, RSC Adv. 8 (2018) 30412–30428, https://doi.org/10.1039/C8RA05007D.

[65] G. Wang, X. Liao, J. Yang, W. Tang, Y. Zhang, Q. Jiang, G. Li, Frequency-selective and tunable electromagnetic shielding effectiveness via the sandwich structure of silicone rubber/graphene composite, Compos. Sci. Technol. 184 (2019) 107847, https://doi.org/10.1016/J.COMPSCITECH.2019.107847.
[66] A.A. Al-Ghamdi, A.A. Al-Ghamdi, Y. Al-Turki, F. Yakuphanoglu, F. El-Tantawy, Electromagnetic shielding properties of graphene/acrylonitrile butadiene rubber nanocomposites for portable and flexible electronic devices, Compos. B Eng. 88 (2016) 212–219, https://doi.org/10.1016/J.COMPOSITESB.2015.11.010.
[67] S.C. Lin, C.C.M. Ma, S.T. Hsiao, Y.S. Wang, C.Y. Yang, W.H. Liao, S.M. Li, J.A. Wang, T.Y. Cheng, C.W. Lin, R. Bin Yang, Electromagnetic interference shielding performance of waterborne polyurethane composites filled with silver nanoparticles deposited on functionalized graphene, Appl. Surf. Sci. 385 (2016) 436–444, https://doi.org/10.1016/J.APSUSC.2016.05.063.
[68] Y. Chen, H. Bin Zhang, Y. Huang, Y. Jiang, W.G. Zheng, Z.Z. Yu, Magnetic and electrically conductive epoxy/graphene/carbonyl iron nanocomposites for efficient electromagnetic interference shielding, Compos. Sci. Technol. 118 (2015) 178–185, https://doi.org/10.1016/J.COMPSCITECH.2015.08.023.
[69] S.P. Pawar, S. Stephen, S. Bose, V. Mittal, Tailored electrical conductivity, electromagnetic shielding and thermal transport in polymeric blends with graphene sheets decorated with nickel nanoparticles, Phys. Chem. Chem. Phys. 17 (2015) 14922–14930, https://doi.org/10.1039/C5CP00899A.
[70] H.J. Im, G.H. Jun, D.J. Lee, H.J. Ryu, S.H. Hong, Enhanced electromagnetic interference shielding behavior of Graphene Nanoplatelet/Ni/Wax nanocomposites, J Mater Chem C Mater 5 (2017) 6471–6479, https://doi.org/10.1039/C7TC01405H.
[71] L. Liang, P. Xu, Y. Wang, Y. Shang, J. Ma, F. Su, Y. Feng, C. He, Y. Wang, C. Liu, Flexible polyvinylidene fluoride film with alternating oriented graphene/Ni nanochains for electromagnetic interference shielding and thermal management, Chem. Eng. J. 395 (2020) 125209, https://doi.org/10.1016/J.CEJ.2020.125209.
[72] B. Zhao, S. Wang, C. Zhao, R. Li, S.M. Hamidinejad, Y. Kazemi, C.B. Park, Synergism between carbon materials and Ni chains in flexible poly(vinylidene fluoride) composite films with high heat dissipation to improve electromagnetic shielding properties, Carbon N Y 127 (2018) 469–478, https://doi.org/10.1016/J.CARBON.2017.11.032.
[73] Z. Guo, P. Ren, B. Fu, F. Ren, Y. Jin, Z. Sun, Multi-layered graphene-Fe3O4/poly (vinylidene fluoride) hybrid composite films for high-efficient electromagnetic shielding, Polym. Test. 89 (2020) 106652, https://doi.org/10.1016/J.POLYMERTESTING.2020.106652.
[74] Y. Chen, Y. Wang, H. Bin Zhang, X. Li, C.X. Gui, Z.Z. Yu, Enhanced electromagnetic interference shielding efficiency of polystyrene/graphene composites with magnetic Fe3O4 nanoparticles, Carbon N Y 82 (2015) 67–76, https://doi.org/10.1016/J.CARBON.2014.10.031.
[75] Y. Liu, M. Lu, K. Wu, S. Yao, X. Du, G. Chen, Q. Zhang, L. Liang, M. Lu, Anisotropic thermal conductivity and electromagnetic interference shielding of epoxy nanocomposites based on magnetic driving reduced graphene oxide@Fe3O4, Compos. Sci. Technol. 174 (2019) 1–10, https://doi.org/10.1016/J.COMPSCITECH.2019.02.005.
[76] Y. Zhan, J. Wang, K. Zhang, Y. Li, Y. Meng, N. Yan, W. Wei, F. Peng, H. Xia, Fabrication of a flexible electromagnetic interference shielding Fe3O4@reduced graphene oxide/natural rubber composite with segregated network, Chem. Eng. J. 344 (2018) 184–193, https://doi.org/10.1016/J.CEJ.2018.03.085.
[77] R.S. Yadav, I. Kuřitka, J. Vilcakova, D. Skoda, P. Urbánek, M. Machovsky, M. Masař, L. Kalina, J. Havlica, Lightweight NiFe2O4-Reduced Graphene Oxide-Elastomer Nanocomposite flexible sheet for electromagnetic interference shielding application, Compos. B Eng. 166 (2019) 95–111, https://doi.org/10.1016/J.COMPOSITESB.2018.11.069.
[78] S. Li, W. Li, J. Nie, D. Liu, G. Sui, Synergistic effect of graphene nanoplate and carbonized loofah fiber on the electromagnetic shielding effectiveness of PEEK-based composites, Carbon N Y 143 (2019) 154–161, https://doi.org/10.1016/J.CARBON.2018.11.015.
[79] A.P. Singh, P. Garg, F. Alam, K. Singh, R.B. Mathur, R.P. Tandon, A. Chandra, S.K. Dhawan, Phenolic resin-based composite sheets filled with mixtures of reduced graphene oxide, γ-Fe2O3 and carbon fibers for excellent electromagnetic interference shielding in the X-band, Carbon N Y 50 (2012) 3868–3875, https://doi.org/10.1016/J.CARBON.2012.04.030.
[80] S. Maiti, B.B. Khatua, Graphene nanoplate and multiwall carbon nanotube–embedded polycarbonate hybrid composites: high electromagnetic interference shielding with low percolation threshold, Polym. Compos. 37 (2016) 2058–2069, https://doi.org/10.1002/PC.23384.
[81] J.H. Lin, Z.I. Lin, Y.J. Pan, C.L. Huang, C.K. Chen, C.W. Lou, Polymer composites made of multi-walled carbon nanotubes and graphene nano-sheets: effects of sandwich structures on their electromagnetic interference shielding effectiveness, Compos. B Eng. 89 (2016) 424–431, https://doi.org/10.1016/J.COMPOSITESB.2015.11.014.
[82] M. Verma, S.S. Chauhan, S.K. Dhawan, V. Choudhary, Graphene nanoplatelets/carbon nanotubes/polyurethane composites as efficient shield against electromagnetic polluting radiations, Compos. B Eng. 120 (2017) 118–127, https://doi.org/10.1016/J.COMPOSITESB.2017.03.068.
[83] S. Zhu, C. Xing, F. Wu, X. Zuo, Y. Zhang, C. Yu, M. Chen, W. Li, Q. Li, L. Liu, Cake-like flexible carbon nanotubes/graphene composite prepared via a facile method for high-performance electromagnetic interference shielding, Carbon N Y 145 (2019) 259–265, https://doi.org/10.1016/J.CARBON.2019.01.030.
[84] H. Jia, Q.Q. Kong, Z. Liu, X.X. Wei, X.M. Li, J.P. Chen, F. Li, X. Yang, G.H. Sun, C.M. Chen, 3D graphene/carbon nanotubes/polydimethylsiloxane composites as high-performance electromagnetic shielding material in X-band, Compos Part A Appl Sci Manuf 129 (2020) 105712, https://doi.org/10.1016/J.COMPOSITESA.2019.105712.
[85] S. Biswas, I. Arief, S.S. Panja, S. Bose, Absorption-dominated electromagnetic wave suppressor derived from ferrite-doped cross-linked graphene framework and conducting carbon, ACS Appl. Mater. Interfaces 9 (2017) 3030–3039, https://doi.org/10.1021/ACSAMI.6B14853/ASSET/IMAGES/LARGE/AM-2016-14853G_0005. JPEG.
[86] S.H. Lee, D. Kang, I.K. Oh, Multilayered graphene-carbon nanotube-iron oxide three-dimensional heterostructure for flexible electromagnetic interference shielding film, Carbon N Y 111 (2017) 248–257, https://doi.org/10.1016/J.CARBON.2016.10.003.
[87] X. Yang, Y. Zhang, J. Luo, R. Tusiime, C. Lu, Y. Xue, J. Zhou, Y. Liu, H. Zhang, J. Yu, Fe3O4 uniformly decorated reduced graphene oxide aerogel for epoxy nanocomposites with high EMI shielding performance, Compos. Commun. 36 (2022) 101391, https://doi.org/10.1016/J.COCO.2022.101391.
[88] R. Bera, A. Maitra, S. Paria, S.K. Karan, A.K. Das, A. Bera, S.K. Si, L. Halder, A. De, B.B. Khatua, An approach to widen the electromagnetic shielding efficiency in PDMS/ferrous ferric oxide decorated RGO–SWCNH composite through pressure induced tunability, Chem. Eng. J. 335 (2018) 501–509, https://doi.org/10.1016/J.CEJ.2017.10.178.
[89] J. Liu, H.-B. Zhang, R. Sun, Y. Liu, Z. Liu, A. Zhou, Z.-Z. Yu, J. Liu, H. Zhang, R. Sun, Y. Liu, Z. Liu, Z. Yu, A. Zhou, Hydrophobic, flexible, and lightweight MXene foams for high-performance electromagnetic-interference shielding, Adv. Mater. 29 (2017) 1702367, https://doi.org/10.1002/ADMA.201702367.
[90] A. Iqbal, F. Shahzad, K. Hantanasirisakul, M.K. Kim, J. Kwon, J. Hong, H. Kim, D. Kim, Y. Gogotsi, C.M. Koo, Anomalous absorption of electromagnetic waves by 2D transition metal carbonitride Ti3CNTx(MXene), Science 369 (2020) (1979) 446–450, https://doi.org/10.1126/SCIENCE.ABA7977/SUPPL_FILE/ABA7977-IQBAL-SM.PDF.
[91] J. Yao, L. Zhang, F. Yang, Z. Jiao, X. Tao, Z. Yao, Y. Zheng, J. Zhou, Superhydrophobic Ti3C2Tx MXene/aramid nanofiber films for high-performance electromagnetic interference shielding in thermal environment, Chem. Eng. J. 446 (2022), https://doi.org/10.1016/j.cej.2022.136945.
[92] M. Ma, X. Liao, Q. Chu, S. Chen, Y. Shi, H. He, X. Wang, Construction of gradient conductivity cellulose nanofiber/MXene composites with efficient electromagnetic interference shielding and excellent mechanical properties, Compos. Sci. Technol. 226 (2022) 109540, https://doi.org/10.1016/J.COMPSCITECH.2022.109540.
[93] Flexible, stretchable and electrically conductive MXene/natural rubber nanocomposite films for efficient electromagnetic interference shielding, Compos. Sci. Technol. 182 (2019) 107754, https://doi.org/10.1016/J.COMPSCITECH.2019.107754.
[94] C. Weng, T. Xing, H. Jin, G. Wang, Z. Dai, Y. Pei, L. Liu, Z. Zhang, Mechanically robust ANF/MXene composite films with tunable electromagnetic interference shielding performance, Compos Part A Appl Sci Manuf 135 (2020) 105927, https://doi.org/10.1016/J.COMPOSITESA.2020.105927.
[95] F. Liu, Y. Li, S. Hao, Y. Cheng, Y. Zhan, C. Zhang, Y. Meng, Q. Xie, H. Xia, Well-aligned MXene/chitosan films with humidity response for high-performance electromagnetic interference shielding, Carbohydr. Polym. 243 (2020) 116467, https://doi.org/10.1016/J.CARBPOL.2020.116467.
[96] Y. Du, J. Xu, J. Fang, Y. Zhang, X. Liu, P. Zuo, Q. Zhuang, Ultralight, highly compressible, thermally stable MXene/aramid nanofiber anisotropic aerogels for electromagnetic interference shielding, J Mater Chem A Mater 10 (2022) 6690–6700, https://doi.org/10.1039/D1TA11025J.
[97] Z. Wang, P. Wang, W. Cao, C. Sun, Z. Song, D. Ji, L. Yang, J. Han, J. Zhu, Robust, transparent, and conductive AgNW/MXene composite polyurethane self-healing film for electromagnetic interference shielding, J Mater Chem C Mater 10 (2022) 17066–17074, https://doi.org/10.1039/D2TC03822F.

[98] S. Lee, M. Kim, V.A. Cao, J. Park, I.J. Yoon, P. Park, J. Nah, High performance flexible electromagnetic interference shielding material realized using ZnO nanorod decorated polyvinylidene fluoride (PVDF)-MXene composite nanofibers, J Mater Chem C Mater 11 (2023) 1522–1529, https://doi.org/10.1039/D2TC04080H.
[99] Z. Liu, W. Wang, J. Tan, J. Liu, M. Zhu, B. Zhu, Q. Zhang, Bioinspired ultra-thin polyurethane/MXene nacre-like nanocomposite films with synergistic mechanical properties for electromagnetic interference shielding, J Mater Chem C Mater 8 (2020) 7170–7180, https://doi.org/10.1039/D0TC01249A.
[100] R. Liu, M. Miao, Y. Li, J. Zhang, S. Cao, X. Feng, Ultrathin biomimetic polymeric Ti 3 C 2 T x MXene composite films for electromagnetic interference shielding, ACS Appl. Mater. Interfaces 10 (2018) 44787–44795, https://doi.org/10.1021/ACSAMI.8B18347/ASSET/IMAGES/LARGE/AM-2018-18347X_0005.JPEG.
[101] W.T. Cao, F.F. Chen, Y.J. Zhu, Y.G. Zhang, Y.Y. Jiang, M.G. Ma, F. Chen, Binary strengthening and toughening of MXene/cellulose nanofiber composite paper with nacre-inspired structure and superior electromagnetic interference shielding properties, ACS Nano 12 (2018) 4583–4593, https://doi.org/10.1021/ACSNANO.8B00997/ASSET/IMAGES/MEDIUM/NN-2018-00997C_M004.GIF.
[102] S. Feng, Z. Zhan, Y. Yi, Z. Zhou, C. Lu, Facile fabrication of MXene/cellulose fiber composite film with homogeneous and aligned structure via wet co-milling for enhancing electromagnetic interference shielding performance, Compos Part A Appl Sci Manuf 157 (2022) 106907, https://doi.org/10.1016/J.COMPOSITESA.2022.106907.
[103] S. Luo, T. Xiang, J. Dong, F. Su, Y. Ji, C. Liu, Y. Feng, A double crosslinking MXene/cellulose nanofiber layered film for improving mechanical properties and stable electromagnetic interference shielding performance, J. Mater. Sci. Technol. 129 (2022) 127–134, https://doi.org/10.1016/J.JMST.2022.04.044.
[104] W. Tao, M. Ma, X. Liao, W. Shao, S. Chen, Y. Shi, H. He, X. Wang, Cellulose nanofiber/MXene/mesoporous carbon hollow spheres composite films with porous structure for deceased reflected electromagnetic interference shielding, Compos. Commun. 41 (2023) 101647, https://doi.org/10.1016/J.COCO.2023.101647.
[105] L. Chen, T. Mai, X.X. Ji, P.L. Wang, M.Y. Qi, Q. Liu, Y. Ding, M.G. Ma, 3D printing of customizable and lightweight multilayer MXene/nanocellulose architectures for tunable electromagnetic interference shielding via direct ink writing, Chem. Eng. J. 476 (2023) 146652, https://doi.org/10.1016/J.CEJ.2023.146652.
[106] L. Wang, L. Chen, P. Song, C. Liang, Y. Lu, H. Qiu, Y. Zhang, J. Kong, J. Gu, Fabrication on the annealed Ti3C2Tx MXene/Epoxy nanocomposites for electromagnetic interference shielding application, Compos. B Eng. 171 (2019) 111–118, https://doi.org/10.1016/J.COMPOSITESB.2019.04.050.
[107] H. Jin, N. Matsuhisa, S. Lee, M. Abbas, T. Yokota, T. Someya, Enhancing the performance of stretchable conductors for E-textiles by controlled ink permeation, Adv. Mater. 29 (2017) 1605848, https://doi.org/10.1002/ADMA.201605848.
[108] L. Hu, M. Pasta, F. La Mantia, L. Cui, S. Jeong, H.D. Deshazer, J.W. Choi, S.M. Han, Y. Cui, Stretchable, porous, and conductive energy textiles, Nano Lett. 10 (2010) 708–714, https://doi.org/10.1021/NL903949M/SUPPL_FILE/NL903949M_SI_001.PDF.
[109] P. Mostafalu, G. Kiaee, G. Giatsidis, A. Khalilpour, M. Nabavinia, M.R. Dokmeci, S. Sonkusale, D.P. Orgill, A. Tamayol, A. Khademhosseini, A textile dressing for temporal and dosage controlled drug delivery, Adv. Funct. Mater. 27 (2017) 1702399, https://doi.org/10.1002/ADFM.201702399.
[110] J. Lee, Y. Liu, Y. Liu, S.J. Park, M. Park, H.Y. Kim, Ultrahigh electromagnetic interference shielding performance of lightweight, flexible, and highly conductive copper-clad carbon fiber nonwoven fabrics, J Mater Chem C Mater 5 (2017) 7853–7861, https://doi.org/10.1039/C7TC02074K.
[111] D. Yao, Z. Tang, Z. Liang, L. Zhang, Q.J. Sun, J. Fan, G. Zhong, Q.X. Liu, Y.P. Jiang, X.G. Tang, V.A.L. Roy, J. Ouyang, Adhesive, multifunctional, and wearable electronics based on MXene-coated textile for personal heating systems, electromagnetic interference shielding, and pressure sensing, J. Colloid Interface Sci. 630 (2023) 23–33, https://doi.org/10.1016/J.JCIS.2022.09.003.
[112] T. Chen, J. Cai, X. Cheng, S. Cui, D. Zhang, D. Gong, Bio-inspired flexible versatile textiles for excellent absorption-dominated electromagnetic interference shielding, thermal management, and strain sensing, Chem. Eng. J. 477 (2023) 147116, https://doi.org/10.1016/J.CEJ.2023.147116.
[113] M. Zhang, M. Wang, M. Zhang, Q. Gao, X. Feng, Y. Zhang, J. Hu, G. Wu, Stretchable conductive Ni@Fe3O4@Polyester fabric strain sensor with negative resistance variation and electromagnetic interference shielding, Org. Electron. 81 (2020) 105677, https://doi.org/10.1016/J.ORGEL.2020.105677.
[114] V.T. Nguyen, B.K. Min, Y. Yi, S.J. Kim, C.G. Choi, MXene(Ti3C2TX)/graphene/PDMS composites for multifunctional broadband electromagnetic interference shielding skins, Chem. Eng. J. 393 (2020) 124608, https://doi.org/10.1016/J.CEJ.2020.124608.
[115] X. Zhu, M. Li, X.F. Zhang, J. Liu, J. Yao, MXene functionalized wood composite films for efficient electromagnetic interference shielding and pressure sensing, Adv Mater Technol (2023) 2301009, https://doi.org/10.1002/ADMT.202301009.
[116] M. Sang, S. Wang, S. Liu, M. Liu, L. Bai, W. Jiang, S. Xuan, X. Gong, A hydrophobic, self-powered, electromagnetic shielding PVDF-based wearable device for human body monitoring and protection, ACS Appl. Mater. Interfaces 11 (2019) 47340–47349, https://doi.org/10.1021/ACSAMI.9B16120/ASSET/IMAGES/LARGE/AM9B16120_0008.JPEG.
[117] Q. Zhang, Q. Liang, Z. Zhang, Z. Kang, Q. Liao, Y. Ding, M. Ma, F. Gao, X. Zhao, Y. Zhang, Electromagnetic shielding hybrid nanogenerator for health monitoring and protection, Adv. Funct. Mater. 28 (2018) 1703801, https://doi.org/10.1002/ADFM.201703801.
[118] X. Zheng, W. Nie, Q. Hu, X. Wang, Z. Wang, L. Zou, X. Hong, H. Yang, J. Shen, C. Li, Multifunctional RGO/Ti3C2Tx MXene fabrics for electrochemical energy storage, electromagnetic interference shielding, electrothermal and human motion detection, Mater. Des. 200 (2021) 109442, https://doi.org/10.1016/J.MATDES.2020.109442.
[119] B. Zhao, X. Zhang, J. Deng, C. Zhang, Y. Li, X. Guo, R. Zhang, Flexible PEBAX/graphene electromagnetic shielding composite films with a negative pressure effect of resistance for pressure sensors applications, RSC Adv. 10 (2020) 1535–1543, https://doi.org/10.1039/C9RA08679J.
[120] C. Liang, Y. Liu, Y. Ruan, H. Qiu, P. Song, J. Kong, H. Zhang, J. Gu, Multifunctional sponges with flexible motion sensing and outstanding thermal insulation for superior electromagnetic interference shielding, Compos Part A Appl Sci Manuf 139 (2020) 106143, https://doi.org/10.1016/J.COMPOSITESA.2020.106143.
[121] L. Wu, L. Wang, Z. Guo, J. Luo, H. Xue, J. Gao, Durable and multifunctional superhydrophobic coatings with excellent joule heating and electromagnetic interference shielding performance for flexible sensing electronics, ACS Appl. Mater. Interfaces 11 (2019) 34338–34347, https://doi.org/10.1021/ACSAMI.9B11895/ASSET/IMAGES/LARGE/AM9B11895_0006.JPEG.
[122] D. Yuan, H. Guo, K. Ke, I. Manas-Zloczower, Recyclable conductive epoxy composites with segregated filler network structure for EMI shielding and strain sensing, Compos Part A Appl Sci Manuf 132 (2020) 105837, https://doi.org/10.1016/J.COMPOSITESA.2020.105837.
[123] H. Jia, X. Yang, Q.Q. Kong, L.J. Xie, Q.G. Guo, G. Song, L.L. Liang, J.P. Chen, Y. Li, C.M. Chen, Free-standing, anti-corrosion, super flexible graphene oxide/silver nanowire thin films for ultra-wideband electromagnetic interference shielding, J Mater Chem A Mater 9 (2021) 1180–1191, https://doi.org/10.1039/D0TA09246K.
[124] J.H. Pu, X.J. Zha, L.S. Tang, L. Bai, R.Y. Bao, Z.Y. Liu, M.B. Yang, W. Yang, Human skin-inspired electronic sensor skin with electromagnetic interference shielding for the sensation and protection of wearable electronics, ACS Appl. Mater. Interfaces 10 (2018) 40880–40889, https://doi.org/10.1021/ACSAMI.8B15809/SUPPL_FILE/AM8B15809_SI_005.AVI.
[125] J. Wu, Y.M. Sun, Z. Wu, X. Li, N. Wang, K. Tao, G.P. Wang, Carbon nanocoil-based fast-response and flexible humidity sensor for multifunctional applications, ACS Appl. Mater. Interfaces 11 (2019) 4242–4251, https://doi.org/10.1021/ACSAMI.8B18599/ASSET/IMAGES/LARGE/AM-2018-18599K_0006.JPEG.
[126] S. Yao, A. Myers, A. Malhotra, F. Lin, A. Bozkurt, J.F. Muth, Y. Zhu, S. Yao, A. Myers, Y. Zhu, A. Malhotra, F. Lin, A. Bozkurt, J.F. Muth, A wearable hydration sensor with conformal nanowire electrodes, Adv Healthc Mater 6 (2017) 1601159, https://doi.org/10.1002/ADHM.201601159.
[127] R.J. Maughan, S.M. Shirreffs, Rehydration and recovery after exercise, Sci. Sports 19 (2004) 234–238, https://doi.org/10.1016/J.SCISPO.2004.05.003.
[128] H.Y.Y. Nyein, M. Bariya, B. Tran, C.H. Ahn, B.J. Brown, W. Ji, N. Davis, A. Javey, A wearable patch for continuous analysis of thermoregulatory sweat at rest, Nat. Commun. 12 (1) (2021) 1–13, https://doi.org/10.1038/s41467-021-22109-z, 12 (2021).
[129] S. Mondal, S.J. Kim, C.G. Choi, Honeycomb-like MoS2 nanotube array-based wearable sensors for noninvasive detection of human skin moisture, ACS Appl. Mater. Interfaces 12 (2020) 17029–17038, https://doi.org/10.1021/ACSAMI.9B22915/SUPPL_FILE/AM9B22915_SI_003.AVI.
[130] M. Naguib, V.N. Mochalin, M.W. Barsoum, Y. Gogotsi, 25th anniversary article: MXenes: a new family of two-dimensional materials, Adv. Mater. 26 (2014) 992–1005, https://doi.org/10.1002/ADMA.201304138.
[131] S. Célérier, S. Hurand, C. Garnero, S. Morisset, M. Benchakar, A. Habrioux, P. Chartier, V. Mauchamp, N. Findling, B. Lanson, E. Ferrage, Hydration of Ti 3 C 2 T x MXene: an interstratification process with major implications on physical properties, Chem. Mater. 31 (2019) 454–461, https://doi.org/10.1021/ACS.CHEMMATER.8B03976/ASSET/IMAGES/MEDIUM/CM-2018-039765_M006.GIF.

[132] M. Ghidiu, J. Halim, S. Kota, D. Bish, Y. Gogotsi, M.W. Barsoum, Ion-exchange and cation solvation reactions in Ti3C2 MXene, Chem. Mater. 28 (2016) 3507–3514, https://doi.org/10.1021/ACS.CHEMMATER.6B01275/ASSET/IMAGES/LARGE/CM-2016-01275U_0008. JPEG.
[133] H. An, T. Habib, S. Shah, H. Gao, A. Patel, I. Echols, X. Zhao, M. Radovic, M.J. Green, J.L. Lutkenhaus, Water sorption in MXene/polyelectrolyte multilayers for ultrafast humidity sensing, ACS Appl. Nano Mater. 2 (2019) 948–955, https://doi.org/10.1021/ACSANM.8B02265/SUPPL_FILE/AN8B02265_SI_002.AVI.
[134] L.X. Liu, W. Chen, H. Bin Zhang, Q.W. Wang, F. Guan, Z.Z. Yu, Flexible and multifunctional silk textiles with biomimetic leaf-like MXene/silver nanowire nanostructures for electromagnetic interference shielding, humidity monitoring, and self-derived hydrophobicity, Adv. Funct. Mater. 29 (2019) 1905197, https://doi.org/10.1002/ADFM.201905197.
[135] M. Fan, X. Xia, S. Li, R. Zhang, L. Wu, M. Qu, P. Tang, Y. Bin, Sustainable bacterial cellulose reinforced carbon nanotube buckypaper and its multifunctionality for electromagnetic interference shielding, Joule heating and humidity sensing, Chem. Eng. J. 441 (2022) 136103, https://doi.org/10.1016/J.CEJ.2022.136103.
[136] J. un Jang, S.O. So, H.G. Jang, J. Kim, M.J. Oh, S.H. Kim, J.T. Lee, S.Y. Kim, Stepwise percolation behavior induced by nano-interconnection in electrical conductivity of polymer composites, Materials Today Physics 38 (2023) 101213, https://doi.org/10.1016/J.MTPHYS.2023.101213.
[137] F. El-Tantawy, Development of novel functional conducting elastomer blends containing butyl rubber and low-density polyethylene for current switching, temperature sensor, and EMI shielding effectiveness applications, J. Appl. Polym. Sci. 97 (2005) 1125–1138, https://doi.org/10.1002/APP.21778.
[138] E.T. Farid, N.A. Aal, A.A. Ai-Ghamdi, E.H. Ei-Mossaiamy, New smart conducting elastomer blends of Bi-based superconductor ceramics nanoparticles reinforced natural rubber/low-density polyethylene for double thermistors, antistatic protectors, and electromagnetic interference shielding effectiveness applications, Polym. Eng. Sci. 49 (2009) 592–601, https://doi.org/10.1002/PEN.21297.
[139] J.H. Cai, J. Li, X.D. Chen, M. Wang, Multifunctional polydimethylsiloxane foam with multi-walled carbon nanotube and thermo-expandable microsphere for temperature sensing, microwave shielding and piezoresistive sensor, Chem. Eng. J. 393 (2020) 124805, https://doi.org/10.1016/J.CEJ.2020.124805.
[140] L. Xing, H. Yang, X. Chen, Y. Wang, D. Sha, G. Chen, T. Xing, Caffeic acid induced in-situ growth of AgNWs on cotton fabric for temperature and pressure sensing and electrical interference shielding, Chem. Eng. J. 471 (2023) 144620, https://doi.org/10.1016/J.CEJ.2023.144620.
[141] W. Zhao, Y. Zheng, J. Qian, Z. Zhaofa, Z. Jin, H. Qiu, C. Zhu, X. Hong, AgNWs/MXene derived multifunctional knitted fabric capable of high electrothermal conversion efficiency, large strain and temperature sensing, and EMI shielding, J. Alloys Compd. 923 (2022) 166471, https://doi.org/10.1016/J.JALLCOM.2022.166471.
[142] X. Jia, B. Shen, L. Zhang, W. Zheng, Waterproof MXene-decorated wood-pulp fabrics for high-efficiency electromagnetic interference shielding and Joule heating, Compos. B Eng. 198 (2020) 108250, https://doi.org/10.1016/J.COMPOSITESB.2020.108250.
[143] J. Xie, Y. Zhang, J. Dai, Z. Xie, J. Xue, K. Dai, F. Zhang, D. Liu, J. Cheng, F. Kang, B. Li, Y. Zhao, L. Lin, Q. Zheng, Multifunctional MoSe2@MXene heterostructure-decorated cellulose fabric for wearable thermal therapy, Small 19 (2023) 2205853, https://doi.org/10.1002/SMLL.202205853.
[144] J. Dong, Y. Peng, J. Long, Y. Zhang, Z. Wang, S. Park, Y. Huang, T. Liu, An all-stretchable, ultraviolet protective, and electromagnetic-interference-free E-textile, Adv. Funct. Mater. 33 (2023) 2308426, https://doi.org/10.1002/ADFM.202308426.
[145] B. Zhou, M. Su, D. Yang, G. Han, Y. Feng, B. Wang, J. Ma, J. Ma, C. Liu, C. Shen, Flexible MXene/silver nanowire-based transparent conductive film with electromagnetic interference shielding and electro-photo-thermal performance, ACS Appl. Mater. Interfaces 12 (2020) 40859–40869, https://doi.org/10.1021/ACSAMI.0C09020/ASSET/IMAGES/LARGE/AM0C09020_0006.JPEG.
[146] J. Wang, X. Ma, J. Zhou, F. Du, C. Teng, Bioinspired, high-strength, and flexible MXene/aramid fiber for electromagnetic interference shielding papers with joule heating performance, ACS Nano 16 (2022) 6700–6711, https://doi.org/10.1021/ACSNANO.2C01323/ASSET/IMAGES/MEDIUM/NN2C01323_M005.GIF.
[147] M. Tian, M. Du, L. Qu, S. Chen, S. Zhu, G. Han, Electromagnetic interference shielding cotton fabrics with high electrical conductivity and electrical heating behavior via layer-by-layer self-assembly route, RSC Adv. 7 (2017) 42641–42652, https://doi.org/10.1039/C7RA08224J.
[148] J. Luo, L. Huo, L. Wang, X. Huang, J. Li, Z. Guo, Q. Gao, M. Hu, H. Xue, J. Gao, Superhydrophobic and multi-responsive fabric composite with excellent electro-photo-thermal effect and electromagnetic interference shielding performance, Chem. Eng. J. 391 (2020) 123537, https://doi.org/10.1016/J.CEJ.2019.123537.
[149] Y. Bai, F. Qin, Y. Lu, Multifunctional electromagnetic interference shielding ternary alloy (Ni-W-P) decorated fabric with wide-operating-range joule heating performances, ACS Appl. Mater. Interfaces 12 (2020) 48016–48026, https://doi.org/10.1021/ACSAMI.0C15134/ASSET/IMAGES/LARGE/AM0C15134_0008.JPEG.
[150] Q.W. Wang, H. Bin Zhang, J. Liu, S. Zhao, X. Xie, L. Liu, R. Yang, N. Koratkar, Z.Z. Yu, Multifunctional and water-resistant MXene-decorated polyester textiles with outstanding electromagnetic interference shielding and joule heating performances, Adv. Funct. Mater. 29 (2019) 1806819, https://doi.org/10.1002/ADFM.201806819.
[151] D. Zhang, W. Song, L. Lv, C. Gao, F. Gao, H. Guo, R. Diao, W. Dai, J. Niu, X. Chen, J. Wei, M. Terrones, Y. Wang, Mono-dispersion decorated ultra-long single-walled carbon nanotube/aramid nanofiber for high-strength electromagnetic interference shielding film with Joule heating properties, Carbon N Y 214 (2023) 118315, https://doi.org/10.1016/J.CARBON.2023.118315.
[152] H. Li, Z.K. Ng, R.Y. Tay, S. Huang, S.H. Tsang, E.H.T. Teo, Flexible graphene/MXene composite thin films for high-performance electromagnetic interference shielding and joule heating, ACS Appl. Nano Mater. 6 (2023) 16730–16739, https://doi.org/10.1021/ACSANM.3C02925/SUPPL_FILE/AN3C02925_SI_001.PDF.
[153] B. Zhou, Z. Li, Y. Li, X. Liu, J. Ma, Y. Feng, D. Zhang, C. He, C. Liu, C. Shen, Flexible hydrophobic 2D Ti3C2Tx-based transparent conductive film with multifunctional self-cleaning, electromagnetic interference shielding and joule heating capacities, Compos. Sci. Technol. 201 (2021) 108531, https://doi.org/10.1016/J.COMPSCITECH.2020.108531.
[154] Y. Han, H. Zhong, N. Liu, Y. Liu, J. Lin, P. Jin, In situ surface oxidized copper mesh electrodes for high-performance transparent electrical heating and electromagnetic interference shielding, Adv Electron Mater 4 (2018) 1800156, https://doi.org/10.1002/AELM.201800156.
[155] Y. Zhan, E. Lago, C. Santillo, A.E. Del Río Castillo, S. Hao, G.G. Buonocore, Z. Chen, H. Xia, M. Lavorgna, F. Bonaccorso, An anisotropic layer-by-layer carbon nanotube/boron nitride/rubber composite and its application in electromagnetic shielding, Nanoscale 12 (2020) 7782–7791, https://doi.org/10.1039/C9NR10672C.
[156] L. Li, Y. Cao, X. Liu, J. Wang, Y. Yang, W. Wang, Multifunctional MXene-based fireproof electromagnetic shielding films with exceptional anisotropic heat dissipation capability and joule heating performance, ACS Appl. Mater. Interfaces 12 (2020) 27350–27360, https://doi.org/10.1021/ACSAMI.0C05692/ASSET/IMAGES/LARGE/AM0C05692_0007.JPEG.
[157] Y. Sun, R. Ding, S.Y. Hong, J. Lee, Y.K. Seo, J. Do Nam, J. Suhr, MXene-xanthan nanocomposite films with layered microstructure for electromagnetic interference shielding and Joule heating, Chem. Eng. J. 410 (2021) 128348, https://doi.org/10.1016/J.CEJ.2020.128348.
[158] C. Liang, K. Ruan, Y. Zhang, J. Gu, Multifunctional flexible electromagnetic interference shielding silver nanowires/cellulose films with excellent thermal management and joule heating performances, ACS Appl. Mater. Interfaces 12 (2020) 18023–18031, https://doi.org/10.1021/ACSAMI.0C04482/ASSET/IMAGES/MEDIUM/AM0C04482_M001.GIF.
[159] J.H. Ha, S.K. Hong, J.K. Ryu, J. Bae, S.H. Park, Development of multi-functional graphene polymer composites having electromagnetic interference shielding and de-icing properties, Polymers 11 (2019) 2101, https://doi.org/10.3390/POLYM11122101, 11 (2019) 2101.
[160] J. Li, Y. Wang, T. Yue, Y. Gao, Y. Shi, J.S. S, … and Technology, undefined 2021, Robust electromagnetic interference shielding, joule heating, thermal conductivity, and anti-dripping performances of polyoxymethylene with uniform, Elsevier (n.d.). https://www.sciencedirect.com/science/article/pii/S0266353821000373?casa_token=WFgxtcZ2jH4AAAAA:9laTpjuddzeSHsR-q_hw-SVD8rNc31XGXv-wwqyNCQi-yb5JroVnzP_cHSoYXQF59z0sohShg (accessed November 1, 2023)..
[161] P. Hu, J. Lyu, C. Fu, W. Bin Gong, J. Liao, W. Lu, Y. Chen, X. Zhang, Multifunctional aramid nanofiber/carbon nanotube hybrid aerogel films, ACS Nano 14 (2020) 688–697, https://doi.org/10.1021/ACSNANO.9B07459/ASSET/IMAGES/LARGE/NN9B07459_0005.JPEG.

[162] Y. Yang, S. Chen, W. Li, P. Li, J. Ma, B. Li, X. Zhao, Z. Ju, H. Chang, L. Xiao, H. Xu, Y. Liu, Reduced graphene oxide conformally wrapped silver nanowire networks for flexible transparent heating and electromagnetic interference shielding, ACS Nano 14 (2020) 8754–8765, https://doi.org/10.1021/ACSNANO.0C03337/ASSET/IMAGES/LARGE/NN0C03337_0005.JPEG.
[163] Z. Lei, K. Zhu, F. Lv, M. Hu, X. Liu, J. Wei, S.S. Lyu, D. chuan Mo, Y. Hu, Aramid nanofiber assisted preparation of 3D-oriented graphite/silicone composite slices with high through-plane thermal conductivity and efficient electromagnetic interference shielding, Compos. Sci. Technol. 243 (2023) 110246, https://doi.org/10.1016/J.COMPSCITECH.2023.110246.
[164] Q. Du, C. Li, C. Liu, L. Cheng, G. Chen, N. Chen, D. Wu, J. Sun, Skeleton designable SGP/EA resin composites with integrated thermal conductivity, electromagnetic interference shielding, and mechanical performances, Compos. Sci. Technol. 229 (2022) 109686, https://doi.org/10.1016/J.COMPSCITECH.2022.109686.
[165] K. Rajavel, S. Luo, Y. Wan, X. Yu, Y. Hu, P. Zhu, R. Sun, C. Wong, 2D Ti3C2Tx MXene/polyvinylidene fluoride (PVDF) nanocomposites for attenuation of electromagnetic radiation with excellent heat dissipation, Compos Part A Appl Sci Manuf 129 (2020) 105693, https://doi.org/10.1016/J.COMPOSITESA.2019.105693.
[166] S.H. Lee, S. Yu, F. Shahzad, W.N. Kim, C. Park, S.M. Hong, C.M. Koo, Density-tunable lightweight polymer composites with dual-functional ability of efficient EMI shielding and heat dissipation, Nanoscale 9 (2017) 13432–13440, https://doi.org/10.1039/C7NR02618H.
[167] M. Fan, R. Chen, Y. Lu, R. Liu, Y. Ma, Q. Zhao, S. Ran, P. Tang, Y. Bin, Flexible microfibrillated cellulose/carbon nanotube multilayered composite films with electromagnetic interference shielding and thermal conductivity, Compos. Commun. 35 (2022) 101293, https://doi.org/10.1016/J.COCO.2022.101293.
[168] X. Zou, M. Zhao, K. Shen, C. Huang, Y. Wu, G. Fang, Cellulose wrapped silver nanowire film with enhanced stability for transparent wearable heating and electromagnetic interference shielding, J. Alloys Compd. 907 (2022) 164360, https://doi.org/10.1016/J.JALLCOM.2022.164360.
[169] Y. Feng, J. Song, G. Han, B. Zhou, C. Liu, C. Shen, Transparent and stretchable electromagnetic interference shielding film with fence-like aligned silver nanowire conductive network, Small Methods 7 (2023) 2201490, https://doi.org/10.1002/SMTD.202201490.
[170] C. Wang, Y. Guo, J. Chen, Y. Zhu, Transparent and flexible electromagnetic interference shielding film based on Ag nanowires/ionic liquids/thermoplastic polyurethane ternary composites, Compos. Commun. 37 (2023) 101444, https://doi.org/10.1016/J.COCO.2022.101444.
[171] W. Zhang, X. Zhang, Z. Wu, K. Abdurahman, Y. Cao, H. Duan, D. Jia, Mechanical, electromagnetic shielding and gas sensing properties of flexible cotton fiber/polyaniline composites, Compos. Sci. Technol. 188 (2020) 107966, https://doi.org/10.1016/J.COMPSCITECH.2019.107966.
[172] X. Jia, B. Shen, L. Zhang, W. Zheng, Construction of shape-memory carbon foam composites for adjustable EMI shielding under self-fixable mechanical deformation, Chem. Eng. J. 405 (2021) 126927, https://doi.org/10.1016/J.CEJ.2020.126927.
[173] W. Cheng, Y. Zhang, Y. Tao, J. Lu, J. Liu, B. Wang, L. Song, G. Jie, Y. Hu, Durable electromagnetic interference (EMI) shielding ramie fabric with excellent flame retardancy and Self-healing performance, J. Colloid Interface Sci. 602 (2021) 810–821, https://doi.org/10.1016/J.JCIS.2021.05.159.
[174] D. Kong, J. Li, A. Guo, X. Xiao, High temperature electromagnetic shielding shape memory polymer composite, Chem. Eng. J. 408 (2021) 127365, https://doi.org/10.1016/J.CEJ.2020.127365.
[175] J. Lu, Y. Zhang, Y. Tao, B. Wang, W. Cheng, G. Jie, L. Song, Y. Hu, Self-healable castor oil-based waterborne polyurethane/MXene film with outstanding electromagnetic interference shielding effectiveness and excellent shape memory performance, J. Colloid Interface Sci. 588 (2021) 164–174, https://doi.org/10.1016/J.JCIS.2020.12.076.
[176] W. Li, Z. Song, Y. He, J. Zhang, Y. Bao, W. Wang, Z. Sun, Y. Ma, Z. Liu, L. Niu, Natural sedimentation-assisted fabrication of Janus functional films for versatile applications in Joule heating, electromagnetic interference shielding and triboelectric nanogenerator, Chem. Eng. J. 455 (2023) 140606, https://doi.org/10.1016/J.CEJ.2022.140606.